Optimal Mollifiers for Spherical Deconvolution

Ralf Hielscher Michael Quellmalz

This paper deals with the inversion of the spherical Funk–Radon transform, and, more generally, with the inversion of spherical convolution operators from the point of view of statistical inverse problems. This means we consider discrete data perturbed by white noise and aim at estimators with optimal mean square error for functions out of a Sobolev ball. To this end we analyze a specific class of estimators built upon the spherical hyperinterpolation operator, spherical designs and the mollifier approach. Eventually, we determine optimal mollifier functions with respect to the noise level, the number of data points and the smoothness of the original function. We complete this paper by providing a fast algorithm for the numerical computation of the estimator, which is based on the fast spherical Fourier transform, and by illustrating our theoretical results with numerical experiments.

Math Subject Classifications. 65T40, 45Q05, 65N21, 44A12, 44A35, 62G05.

Keywords and Phrases. Spherical Radon transform, spherical deconvolution, statistical inverse problems, minimax risk, asymptotic bounds, fast algorithms.

1 Introduction

Reconstructing functions defined on the two-sphere $\mathbb{S}^2 = \{\boldsymbol{\xi} \in \mathbb{R}^3 \mid \|\boldsymbol{\xi}\| = 1\}$ from integrals along great circles has been investigated at least since the work of Funk [8], who proved that the so-called Funk–Radon transform

$$\mathcal{F}\colon C(\mathbb{S}^2) \to C(\mathbb{S}^2), \qquad \mathcal{F}(\boldsymbol{\xi}) = \int_{\boldsymbol{\eta}\cdot\boldsymbol{\xi}=0} f(\boldsymbol{\eta})\,\mathrm{d}\boldsymbol{\eta} \tag{1.1}$$

restricted to the space of even, continuous functions on the sphere is injective. Explicit inversion formulas can be found e.g. in [14, Section III.1.A]. For the reconstruction from discrete data $g_m = \mathcal{F}f(\boldsymbol{\xi}_m) + \varepsilon_m$ at points $\boldsymbol{\xi}_m \in \mathbb{S}^2$, $m = 1, \dots, M$, corrupted by white noise ε_m, Louis et. al. [24] proposed a mollifier-based approach. Explicit formulas for locally supported mollifiers were discussed in [29]. The latter two paper include also a complete error analysis in the Sobolev scale as well as explicit numerical algorithms and numerical tests. An approach based on variational splines was suggested by Pesenson [26].

Technische Universität Chemnitz, Faculty of Mathematics, 09107 Chemnitz, Germany, mails ralf.hielscher@mathematik.tu-chemnitz.de, michael.quellmalz@mathematik.tu-chemnitz.de

In this paper we aim at optimal mollifiers which take into account the number and the alignment of the evaluation points $\boldsymbol{\xi}_m \in \mathbb{S}^2$, the smoothness of the function f as well as the noise level. To impose a condition on the smoothness of f, we consider Sobolev balls which are sets of even functions $f \in H^s_{\mathrm{e}}(\mathbb{S}^2)$ with bounded Sobolev norm $\|f\|_{H^s} \leq S$ for some $s, S > 0$. As measure of optimality of a fixed mollifier ψ, we use the maximum risk

$$\sup_{\substack{f \in H^s_{\mathrm{e}}(\mathbb{S}^2) \\ \|f\|_{H^s} \leq S}} \mathbb{E}\, \|f - \mathcal{E}_\psi(\mathcal{F}f + \varepsilon)\|_{L^2}^2\,, \tag{1.2}$$

where $\mathcal{E}_\psi(\mathcal{F}f+\varepsilon)$ denotes the reconstruction of f using the mollifier ψ and where the expected value $\mathbb{E}$ is with respect to the white noise ε.

The approach taken in this paper is entirely based on Fourier series with respect to spherical harmonics (cf. [16] for the Fourier approach in $\mathbb{R}^d$). We make use of the fact that the Funk–Radon transform is a multiplication operator in Fourier space and that it suffices to specify the mollifier by its Fourier coefficients. The advantages of this approach are as follows. Firstly, we are not restricted to specific mollifiers which are Funk–Radon transforms of approximating identities. Secondly, the estimator $\mathcal{E}_\psi(\mathcal{F}f + \varepsilon)$, the Sobolev norm $\|f\|_{H^s}$ and the maximum risk (1.2) can be easily expressed with respect to the Fourier coefficients of f. Lastly, this representation leads to a fast inversion algorithm, i.e. an algorithm that scales like $\mathcal{O}(M \log M)$, by applying the nonequispaced fast spherical Fourier transform [17, 22].

Similarly to the work of Kim and Koo [19], who investigated the maximum risk for density estimation on the sphere from random samples, we formulate our results directly for spherical Fourier multiplication operators, which are a generalization of spherical convolution operators. Besides the Funk–Radon transform, which is important e.g. for Q–ball imaging [34], radar imaging [35] and geometric tomography [10, Chap. 4]; spherical Fourier multiplication operators also include the spherical cosine transform [28]

$$\mathcal{C}\colon C(\mathbb{S}^2) \to C(\mathbb{S}^2), \qquad \mathcal{C}f(\boldsymbol{\xi}) = \int_{\mathbb{S}^2} |\boldsymbol{\xi} \cdot \boldsymbol{\eta}|\, f(\boldsymbol{\eta})\, \mathrm{d}\boldsymbol{\eta}, \tag{1.3}$$

whose inversion is important for the analysis of fiber systems [18] and was subject of the papers [33, 24, 29], and the hemispherical transform [9] (see also [3, 32]), which has applications for discrete choice models [11].

This paper is organized as follows. In Section 2 we set up notation for harmonic analysis on the sphere and cite results about hyperinterpolation on the sphere from [15]. In Section 3, Equation (3.1), we define a family of estimators $\mathcal{E}_\psi$, which use hyperinterpolation to estimate Fourier coefficients out of the data g_m and then utilize the Funk–Hecke formula for the convolution with the mollifier ψ. In Definition 3.3 we define a special class of mollifiers $\psi^s_{\tilde{N}}$, adapted to the Sobolev space $H^s(\mathbb{S}^2)$, and show in Lemma 3.4 that this class provides a lower bound of the maximum risk (1.2) amongst all mollifiers. By optimizing with respect to the parameter $\tilde{N}$ of this class, we obtain in Theorem 3.6 a lower bound of the maximum risk over Sobolev balls. In Theorem 3.9 we prove an upper bound, which has the same asymptotic rate in the number M of data points as the lower bound. Theorem 3.10 gives sufficient conditions that the upper and lower bounds have the same constants. In Corollary 3.11 we specialize our findings for the case of the Funk–Radon and the cosine transform, for which we give explicit error rates and formulas for optimal mollifiers.

Section 4 is devoted to numerical experiments in order to illustrate the theoretical findings of the previous sections. First we present in Section 4.1 fast algorithms for the forward transform

as well as for the inverse transform which make use of spherical quadrature rules [13] and the nonequispaced fast spherical Fourier transform [17, 21]. The numerical complexity of this algorithm is $\mathcal{O}(M \log^2 M + J)$, where M denotes the number of sampling points and J the number of points where the estimator is evaluated.

In Section 4.3 we compare our algorithm with the algorithm suggested in [29] using locally supported mollifiers. Although, as expected, the optimal mollifier achieves a slightly better L^2–error, the visual difference between both reconstructions is negligible. The main disadvantage of the locally supported mollifiers is that the corresponding reconstruction kernels are not longer locally supported but supported on the entire two-dimensional sphere. Hence, computing the convolutions between the data and the reconstruction kernel directly yields the numerical complexity $\mathcal{O}(MJ)$. These additional expenses compared to the Fourier-based algorithm show up in the numerical experiments already for small numbers of sampling points.

We proceed in Section 4.3 as well as in Section 4.4 by analyzing the rate of decay of the mean reconstruction error for a specific test function with respect to the number of sampling points. The numerical results fit well with the asymptotic rates obtained in Corollary 3.11.

2 Approximation on the Sphere

2.1 Spherical Harmonics

In this section we are going to summarize some basic facts on harmonic analysis on the sphere as it can be found, e.g., in [7, 5]. We define the two-dimensional sphere $\mathbb{S}^2 = \{\boldsymbol{\xi} \in \mathbb{R}^3 \mid |\boldsymbol{\xi}| = 1\}$ as the set of unit vectors in the three-dimensional Euclidean space and make use of its parametrization in terms of polar angles

$$\boldsymbol{\xi}(\theta, \rho) = (\cos\rho \sin\theta, \sin\rho \sin\theta, \cos\theta)^t, \quad \theta \in [0, \pi],\ \rho \in [0, 2\pi).$$

With respect to polar angles, the surface measure $\mathrm{d}\boldsymbol{\xi}$ on the sphere reads as

$$\int_{\mathbb{S}^2} f(\boldsymbol{\xi}) \,\mathrm{d}\boldsymbol{\xi} = \int_0^{\pi} \int_0^{2\pi} f(\boldsymbol{\xi}(\theta, \rho)) \,\mathrm{d}\rho \sin\theta \,\mathrm{d}\theta,$$

where $f\colon \mathbb{S}^2 \to \mathbb{C}$ is some measurable function. The Hilbert space $L^2(\mathbb{S}^2)$ is the space of all measurable functions $f\colon \mathbb{S}^2 \to \mathbb{C}$, whose norm $\|f\|_{L^2} = \sqrt{\int_{\mathbb{S}^2} |f(\boldsymbol{\xi})|^2 \,\mathrm{d}\boldsymbol{\xi}}$ is finite.

We define the associated Legendre polynomials

$$P_n^k(t) = \frac{(-1)^k}{2^k k!} \left(1 - t^2\right)^{k/2} \frac{\mathrm{d}^{n+k}}{\mathrm{d}t^{n+k}} \left(t^2 - 1\right)^k, \quad t \in [-1, 1],$$

for all

$$(n, k) \in I := \{(n, k) \mid n \in \mathbb{N}, k = -n, \ldots, n\}.$$

For $k = 0$, they are equal to the Legendre polynomials $P_n = P_n^0$. An orthonormal basis in the Hilbert space $L^2(\mathbb{S}^2)$ of square integrable functions on the sphere is formed by the so-called spherical harmonics

$$Y_n^k(\boldsymbol{\xi}(\theta, \rho)) = \sqrt{\frac{2n+1}{4\pi} \frac{(n-k)!}{(n+k)!}}\, P_n^k(\cos\theta) \mathrm{e}^{\mathrm{i}k\rho}, \quad (n, k) \in I.$$

Accordingly, a function $f \in L^2(\mathbb{S}^2)$ can be expressed by its Fourier series

$$f = \sum_{(n,k)\in I} \hat{f}(n,k) Y_n^k$$

with Fourier coefficients

$$\hat{f}(n,k) = \int_{\mathbb{S}^2} f(\boldsymbol{\xi}) \overline{Y_n^k(\boldsymbol{\xi})} \, \mathrm{d}\boldsymbol{\xi}, \quad (n,k) \in I.$$

A function $p\colon \mathbb{S}^2 \to \mathbb{C}$ that has a finite representation

$$p = \sum_{(n,k)\in I_N} \hat{p}(n,k) Y_n^k, \quad I_N = \{(n,k) \in I \mid n \le N\},$$

with respect to spherical harmonics is called a spherical polynomial of degree $N \in \mathbb{N}$ provided that $\hat{p}(N,k) \neq 0$ for some k. We denote by $\Pi_N(\mathbb{S}^2)$ the space of all spherical polynomials of degree up to N. For a spherical polynomial $p \in \Pi_N(\mathbb{S}^2)$ and some $s \in \mathbb{R}$ we introduce the Sobolev norm

$$\|p\|_{H^s}^2 = \sum_{(n,k)\in I_N} (n+\tfrac{1}{2})^{2s} \left|\hat{p}(n,k)\right|^2.$$

As usual the spherical Sobolev spaces $H^s(\mathbb{S}^2)$, cf. [7], are defined as the completion of the space of all spherical polynomials with respect to the Sobolev norm $\|\cdot\|_{H^s}$.

2.2 Spherical convolution and Fourier multiplication operators

It is well known that the Legendre polynomials P_n of degree $n \in \mathbb{N}$ form a system of orthogonal polynomials in $L^2([-1,1])$. They satisfy the three-term recurrence relation

$$P_n(t) = \frac{2n-1}{n} t P_{n-1}(t) - \frac{n-1}{n} P_{n-2}(t), \quad t \in [-1,1], \tag{2.1}$$

for $n \ge 1$ with the initialization $P_0(t) \equiv 1$ and $P_{-1}(t) \equiv 0$. For a function $\psi \in L^2([-1,1])$, we consider its expansion into a Legendre series

$$\psi = \sum_{n=0}^{\infty} \frac{2n+1}{4\pi} \hat{\psi}(n) P_n$$

with the Legendre coefficients

$$\hat{\psi}(n) = 2\pi \int_{-1}^{1} \psi(t) P_n(t) \, \mathrm{d}t.$$

The convolution of $\psi \in L^2([-1,1])$ with a spherical function $f \in L^2(\mathbb{S}^2)$ is defined as

$$\psi \star f(\boldsymbol{\xi}) = \int_{\mathbb{S}^2} f(\boldsymbol{\eta}) \, \psi(\boldsymbol{\xi} \cdot \boldsymbol{\eta}) \, \mathrm{d}\eta.$$

Using the addition Theorem, cf. [25],

$$(2n+1) P_n(\boldsymbol{\xi} \cdot \boldsymbol{\eta}) = 4\pi \sum_{k=-n}^{n} Y_n^k(\boldsymbol{\xi}) \overline{Y_n^k(\boldsymbol{\eta})}, \tag{2.2}$$

we obtain the spherical convolution theorem

$$\widehat{\psi \star f}(n,k) = \hat{\psi}(n)\hat{f}(n,k). \tag{2.3}$$

As a generalization of spherical convolution operators $\mathcal{M}_\psi : C(\mathbb{S}^2) \to C(\mathbb{S}^2),\ f \mapsto \psi \star f$, we define Fourier multiplication operators.

Definition 2.1. Let $\beta \in \mathbb{R}$ and let $\hat{\mathcal{M}}(n) \in \mathbb{R}$, $n = 0, \dots, \infty$, be a sequence such that $n^\beta \hat{\mathcal{M}}(n)$ is bounded uniformly for all $n \in \mathbb{N}$. Then the Fourier multiplication operator $\mathcal{M}$ with symbol $\hat{\mathcal{M}}$ is defined as the operator

$$\mathcal{M}\colon H^0(\mathbb{S}^2) \to H^\beta(\mathbb{S}^2), \quad \mathcal{M}f = \sum_{(n,k)\in I} \hat{\mathcal{M}}(n)\hat{f}(n,k)Y_n^k.$$

The generalized inverse $\mathcal{M}^+$ of $\mathcal{M}$ is defined as the Fourier multiplication operator with symbol $\hat{\mathcal{M}}$ given by

$$\hat{\mathcal{M}}^+(n) = \begin{cases} 0, & \text{if } \hat{\mathcal{M}}(n) = 0, \\ \hat{\mathcal{M}}(n)^{-1}, & \text{otherwise.} \end{cases}$$

Since we have assumed that the symbol only contains of real numbers, $\mathcal{M}$ is a self-adjoint operator. Obviously, $\mathcal{M}\colon H^0(\mathbb{S}^2) \to H^\beta(\mathbb{S}^2)$ is bounded with norm

$$\|\mathcal{M}\|_{H^0\to H^\beta} = \sup_{n\in\mathbb{N}} (n+\tfrac{1}{2})^\beta \left|\hat{\mathcal{M}}(n)\right|.$$

If $\mathcal{M}\colon H^0(\mathbb{S}^2) \to H^\beta(\mathbb{S}^2)$ is also open, then it is invertible with $\mathcal{M}^{-1} = \mathcal{M}^+$ and its symbol $\hat{\mathcal{M}}(n)$ is bounded for all $n \in \mathbb{N}$ by

$$\|\mathcal{M}^+\|^{-1}_{H^\beta\to H^0} \le (n+\tfrac{1}{2})^\beta \left|\hat{\mathcal{M}}(n)\right| \le \|\mathcal{M}\|_{H^0\to H^\beta}. \tag{2.4}$$

Important examples of Fourier multiplication operators are the Funk–Radon transform as defined in (1.1) as well as the spherical cosine transform from (1.3). The corresponding symbols are well-known, cf. e.g. [8] and [31], respectively.

Lemma 2.2. *Let $s \in \mathbb{R}$. The Funk–Radon transform $\mathcal{F}\colon H^s(\mathbb{S}^2) \to H^{s+\frac{1}{2}}(\mathbb{S}^2)$ is a bounded Fourier multiplication operator with symbol*

$$\hat{\mathcal{F}}(n) = \begin{cases} (-1)^{n/2}\frac{(n-1)!!}{n!!}, & n \text{ even} \\ 0, & n \text{ odd,} \end{cases}$$

which satisfies

$$\left|\hat{\mathcal{F}}(n)\right| = \sqrt{\frac{2}{\pi}} n^{-\frac{1}{2}} \left(1 + \mathcal{O}\left(\frac{1}{n}\right)\right), \quad n \to \infty,\ n \text{ even.}$$

The spherical cosine transform $\mathcal{C}\colon H^s(\mathbb{S}^2) \to H^{s+\frac{5}{2}}(\mathbb{S}^2)$ is a bounded Fourier multiplication operator with symbol

$$\hat{\mathcal{C}}(0) = 2\pi,\ \hat{\mathcal{C}}(1) = 0, \qquad \hat{\mathcal{C}}(n) = \frac{4\pi}{(n-1)(n+2)}\hat{\mathcal{F}}(n), \quad n \ge 2, \tag{2.5}$$

which satisfies

$$\left|\hat{\mathcal{C}}(n)\right| = 4\sqrt{2\pi} n^{-\frac{5}{2}} \left(1 + \mathcal{O}\left(\frac{1}{n}\right)\right), \quad n \to \infty,\ n \text{ even.}$$

Proof. First of all we note that by the Funk–Hecke formula $\mathcal{F}Y_n^k(\boldsymbol{\xi}) = P_n(0)Y_n^k(\boldsymbol{\xi})$. Using the three-term recurrence relation (2.1) of the Legendre polynomials P_n, we obtain for $n \geq 1$,

$$\hat{\mathcal{F}}(n) = P_n(0) = \frac{-(n-1)P_{n-2}(0)}{n} = \begin{cases} (-1)^{n/2}\frac{(n-1)!!}{n!!}, & n \text{ even} \\ 0, & n \text{ odd.} \end{cases}$$

For a polynomial bound of $\left|\hat{\mathcal{F}}(n)\right|$, $n \in 2\mathbb{N}$, we make use of the following version of Stirling's formula, cf. [30],

$$\sqrt{2\pi}n^{n+\frac{1}{2}}\mathrm{e}^{-n+\frac{1}{12n+1}} < n! < \sqrt{2\pi}n^{n+\frac{1}{2}}\mathrm{e}^{-n+\frac{1}{12n}},$$

and we find out that $|P_n(0)| = \frac{n!}{2^n(\frac{n}{2}!)^2}$ can be bounded from above and below by

$$\begin{aligned} \frac{\sqrt{2\pi}n^{n+\frac{1}{2}}\mathrm{e}^{-n+\frac{1}{12n+1}}}{2^n 2\pi(\frac{n}{2})^{n+1}\mathrm{e}^{-n+\frac{4}{12n}}} &< \left|\hat{\mathcal{F}}(n)\right| < \frac{\sqrt{2\pi}n^{n+\frac{1}{2}}\mathrm{e}^{-n+\frac{1}{12n}}}{2^n 2\pi(\frac{n}{2})^{n+1}\mathrm{e}^{-n+\frac{2}{12n/2+1}}} \\ \frac{\sqrt{2}}{\sqrt{\pi n}}\mathrm{e}^{\frac{1}{12n+1}-\frac{1}{3n}} &< \left|\hat{\mathcal{F}}(n)\right| < \frac{\sqrt{2}}{\sqrt{\pi n}}\mathrm{e}^{\frac{1}{12n}-\frac{1}{12n+1/2}} \\ \frac{\sqrt{2}}{\sqrt{\pi n}}\mathrm{e}^{\frac{1-9n}{(12n+1)3n}} &< \left|\hat{\mathcal{F}}(n)\right| < \frac{\sqrt{2}}{\sqrt{\pi n}}\mathrm{e}^{\frac{1}{24n(12n+1/2)}}. \end{aligned}$$

Using the Taylor expansion of the exponential function we conclude for $n \to \infty$ and n even,

$$\left|\hat{\mathcal{F}}(n)\right| = \frac{\sqrt{2}}{\sqrt{\pi n}}\left(1 + \mathcal{O}\left(\frac{1}{n}\right)\right),$$

which proves that the Funk–Radon transform extends to a bounded operator $\mathcal{F}\colon H^s(\mathbb{S}^2) \to H^{s+\frac{1}{2}}(\mathbb{S}^2)$.

In the second part of the proof, we compute the symbol $\hat{\mathcal{C}}$ of the cosine transform. The Funk–Radon and cosine transform are related via the equation [12]

$$\mathcal{F} = \frac{\Delta_0 + 2}{4\pi}\mathcal{C},$$

where Δ_0 denotes the Laplace-Beltrami operator. Making use of the fact that the spherical harmonics Y_n^k are eigenfunctions of the Laplace-Beltrami operator, i.e. $\Delta_0 Y_n^k = -n(n+1)Y_n^k$ for all $(n,k) \in I$, we observe that

$$\frac{\Delta_0 + 2}{4\pi}Y_n^k = \frac{-n(n+1)+2}{4\pi}Y_n^k = \frac{-(n+2)(n-1)}{4\pi}Y_n^k, \quad (n,k) \in I.$$

This shows the second part of (2.5). The symbol for $n = 0, 1$ can be simply calculated. ∎

Remark 2.3. Let $\Psi\colon [-1,1] \to \mathbb{R}$ be a polynomial of degree N and let $\boldsymbol{\xi} \in \mathbb{S}^2$. Then $\Psi_{\boldsymbol{\xi}}(\boldsymbol{\eta}) = \Psi(\boldsymbol{\xi}\cdot\boldsymbol{\eta})$, $\boldsymbol{\eta} \in \mathbb{S}^2$, defines a radially symmetric function on the sphere with the center $\boldsymbol{\xi}$. The application of a Fourier multiplication operator $\mathcal{M}$ yields

$$\begin{aligned} \mathcal{M}\Psi(\boldsymbol{\eta}\cdot\circ) &= \sum_{n=0}^{N}\frac{2n+1}{4\pi}\hat{\Psi}(n)\mathcal{M}P_n(\boldsymbol{\eta}\cdot\circ) = \sum_{n=0}^{N}\hat{\Psi}(n)\sum_{k=-n}^{n}\overline{Y_n^k(\boldsymbol{\eta})}\mathcal{M}Y_n^k(\circ) \\ &= \sum_{n=0}^{N}\hat{\mathcal{M}}(n)\hat{\Psi}(n)\sum_{k=-n}^{n}\overline{Y_n^k(\boldsymbol{\eta})}Y_n^k(\circ) = \sum_{n=0}^{N}\frac{2n+1}{4\pi}\hat{\mathcal{M}}(n)\hat{\Psi}(n)P_n(\boldsymbol{\eta}\cdot\circ) =: \psi(\boldsymbol{\eta}\cdot\circ), \end{aligned}$$

which is again a radially symmetric spherical polynomial of degree N. The so-defined polynomial ψ has the Legendre coefficients $\hat{\psi}(n) = \hat{\mathcal{M}}(n)\hat{\Psi}(n)$, $n \in \mathbb{N}$. We shall write $\psi = \mathcal{M}\Psi$ whenever it does not cause confusion. □

2.3 Quadrature and Hyperinterpolation

In this section, we introduce a spherical analogue to the discrete Fourier transform on the torus. To this end, we consider for a finite sequence $\Xi = (\boldsymbol{\xi}_1, \dots, \boldsymbol{\xi}_M)$ of sampling points $\boldsymbol{\xi}_m \in \mathbb{S}^2$, $m = 1, \dots, M$, and positive quadrature weights $\Omega = (\omega_1, \dots, \omega_M) \in \mathbb{R}_+^M$ the quadrature rule

$$Q_{\Xi,\Omega} f = \sum_{m=1}^{M} \omega_m f(\boldsymbol{\xi}_m), \quad f \in C\left(\mathbb{S}^2\right). \tag{2.6}$$

We call the quadrature rule $Q_{\Xi,\Omega}$ exact of degree $N \in \mathbb{N}$ if for all polynomials $p \in \Pi_N(\mathbb{S}^2)$ we have

$$Q_{\Xi,\Omega} p = \int_{\mathbb{S}^2} p(\boldsymbol{\xi}) \, \mathrm{d}\boldsymbol{\xi}. \tag{2.7}$$

In the particular case of constant quadrature weights $\omega_m = 4\pi/M$, an exact quadrature rule of degree N is called a spherical N-design. The existence of spherical N-designs for arbitrary polynomial degree with $M \sim N^2$ quadrature points has been proven in [2]. The numerical computation of spherical N-designs has been analyzed in [13]. The algorithm presented in this paper allows for the stable and efficient computation of spherical N-designs up to polynomial degree $N \approx 1000$ and requires a very small oversampling factor, i.e., $2M \approx 1.04N^2$.

For arbitrary quadrature nodes $\boldsymbol{\xi}_1, \dots, \boldsymbol{\xi}_M \in \mathbb{S}^2$ satisfying for some sufficiently small $\rho > 0$

- $|\boldsymbol{\xi}_m - \boldsymbol{\xi}_l| \geq \rho$ for any $m, l \in \{1, \dots, M\}$ with $m \neq l$, and
- for every $\boldsymbol{\xi} \in \mathbb{S}^2$, there exists an $m \in \{1, \dots, M\}$ such that $|\boldsymbol{\xi} - \boldsymbol{\xi}_m| \leq 2\rho$,

one can ensure the existence of positive quadrature weights ω_m with

$$\delta_1 \frac{4\pi}{M} \leq \omega_m \leq \delta_2 \frac{4\pi}{M} \tag{2.8}$$

for all $m \in \{1, \dots, M\}$ such that the corresponding quadrature rule is exact of degree $N \sim cM^{1/2}$, where the positive constants δ_1, δ_2, and c are independent of M, cf. [6, 27].

For a quadrature rule $Q_{\Xi,\Omega}$ that is exact for polynomials of degree at most $2N$, we define a spherical analogue to the trigonometric interpolation operator, namely

$$\mathcal{L}_N f = \sum_{(n,k) \in I_N} \left(\sum_{m=1}^{M} \omega_m f(\boldsymbol{\xi}_m) \, \overline{Y_{n,k}}(\boldsymbol{\xi}_m) \right) Y_{n,k}, \quad f \in C(\mathbb{S}^2). \tag{2.9}$$

Obviously, $\mathcal{L}_N$ is a projection operator, i.e., $\mathcal{L}_N p = p$ for all $p \in \Pi_N(\mathbb{S}^2)$. But in contrast to the trigonometric case, it is not an interpolation operator for $N \geq 3$. In [15] this operator is called hyperinterpolation and the following approximation result is shown.

Theorem 2.4. *Let $Q_{\Xi,\Omega}$ be a quadrature formula on the sphere, which is exact for polynomial degree $2N$ and let $\mathcal{L}_N$ denote the respective hyperinterpolation. Then, for $t \geq s \geq 0$ with $t > 1$, there is a constant $c > 0$ independent of N such that for any $f \in H^t(\mathbb{S}^2)$ we have the following estimate*

$$\left(N + \frac{1}{2}\right)^{t-s-1} \|\mathcal{L}_N f - f\|_{H^s} \leq c \min_{p \in \Pi_N(\mathbb{S}^2)} \|f - p\|_{H^t} \leq c \|f\|_{H^t}. \tag{2.10}$$

3 Spherical Deconvolution

3.1 The mollifier approach

Let $s + \beta > 1$, $f \in H^s(\mathbb{S}^2)$ and $\mathcal{M}\colon H^s(\mathbb{S}^2) \to H^{s+\beta}(\mathbb{S}^2)$ be a spherical Fourier multiplication operator. We are concerned with the reconstruction of f from sampling values

$$g_m^\varepsilon = \mathcal{M}f(\boldsymbol{\xi}_m) + \varepsilon_m, \quad m = 1, \ldots, M,$$

of the function $g = \mathcal{M}f$ at sampling points $\boldsymbol{\xi}_1, \ldots, \boldsymbol{\xi}_M \in \mathbb{S}^2$ at the presence of white noise ε_m, $m = 1, \ldots, M$ with variance σ^2. We assume this random vector to be derived from a white noise random field ε defined on the sphere, i.e. $\varepsilon_m = \varepsilon(\boldsymbol{\xi}_m)$.

Following the mollifier idea, cf. [23], we consider polynomials $\psi, \Psi\colon [-1, 1] \to \mathbb{R}$ of degree N with $\mathcal{M}\Psi = \psi$ as in Remark 2.3, and aim at computing the convolution

$$\psi \star f(\boldsymbol{\xi}) = \int_{\mathbb{S}^2} f(\boldsymbol{\eta})\, \psi(\boldsymbol{\eta} \cdot \boldsymbol{\xi})\, \mathrm{d}\boldsymbol{\eta} = \int_{\mathbb{S}^2} f(\boldsymbol{\eta})\, \mathcal{M}\Psi(\boldsymbol{\eta} \cdot \boldsymbol{\xi})\, \mathrm{d}\boldsymbol{\eta} = \int_{\mathbb{S}^2} \mathcal{M}f(\boldsymbol{\eta})\, \Psi(\boldsymbol{\eta} \cdot \boldsymbol{\xi})\, \mathrm{d}\boldsymbol{\eta}$$

for $\boldsymbol{\xi} \in \mathbb{S}^2$. For the last equality, we have used the self-adjointness of $\mathcal{M}$. Replacing the integral by a quadrature rule $Q_{\Xi,\Omega}$, with sampling points $\Xi = \{\boldsymbol{\xi}_1, \ldots, \boldsymbol{\xi}_M\}$ and weights $\Omega = (\omega_1, \ldots, \omega_M) \in \mathbb{R}_+^M$, that is exact for polynomials of degree at most $2N$, we end up with the estimator

$$\mathcal{E}_{N,\psi}(\mathcal{M}f) := \sum_{m=1}^{M} \omega_m \mathcal{M}f(\boldsymbol{\xi}_m) \Psi(\boldsymbol{\xi}_m \cdot \circ). \tag{3.1}$$

Next we rewrite the estimator $\mathcal{E}_{N,\psi}$ by using the hyperinterpolation operator $\mathcal{L}_N$, which was defined in (2.9).

Lemma 3.1. *Let $g\colon \mathbb{S}^2 \to \mathbb{C}$ be a function on the sphere. Then*

$$\mathcal{E}_{N,\psi} g = \psi \star \mathcal{M}^+ \mathcal{L}_N g.$$

Proof. For any $\boldsymbol{\xi} \in \mathbb{S}^2$ we obtain

$$\begin{aligned}
\mathcal{E}_{N,\psi} g(\boldsymbol{\xi}) &= \sum_{m=1}^{M} \omega_m g(\boldsymbol{\xi}_m) \Psi(\boldsymbol{\xi}_m \cdot \boldsymbol{\xi}) \\
&= \sum_{m=1}^{M} \omega_m g(\boldsymbol{\xi}_m) \sum_{n=0}^{N} \hat{\mathcal{M}}^+(n) \hat{\psi}(n) \sum_{k=-n}^{n} \overline{Y_n^k(\boldsymbol{\xi}_m)} Y_n^k(\boldsymbol{\xi}) \\
&= \sum_{n=0}^{N} \hat{\mathcal{M}}^+(n) \hat{\psi}(n) \sum_{k=-n}^{n} \left(\sum_{m=1}^{M} \omega_m g(\boldsymbol{\xi}_m) \overline{Y_n^k(\boldsymbol{\xi}_m)} \right) Y_n^k(\boldsymbol{\xi}) \\
&= \psi \star \mathcal{M}^+ \mathcal{L}_N\, g(\boldsymbol{\xi}),
\end{aligned}$$

where the second equality follows from Remark 2.3. ∎

The minimax error. As a measure for the accuracy of the estimator $\mathcal{E}_{N,\psi}$, we consider the mean integrated squared error (MISE)

$$\mathbb{E}\,\|f - \mathcal{E}_{N,\psi}(\mathcal{M}f + \varepsilon)\|_{L^2}^2 = \mathbb{E}\int_{\mathbb{S}^2} |f(\boldsymbol{\eta}) - \mathcal{E}_{N,\psi}(\mathcal{M}f + \varepsilon)(\boldsymbol{\eta})|^2 \,\mathrm{d}\boldsymbol{\eta}, \tag{3.2}$$

or, more specifically, the maximum risk of the MISE over Sobolev balls with degree s and radius S, i.e.

$$\sup_{\substack{f \in H^s(\mathbb{S}^2) \\ \|f\|_{H^s} \leq S}} \mathbb{E}\,\|f - \mathcal{E}_{N,\psi}(\mathcal{M}f + \varepsilon)\|_{L^2}^2 .$$

Note that this definition of the maximum risk only makes sense if the operator $\mathcal{M}$ is open. Otherwise, if the nullspace of $\mathcal{M}$ is non-trivial, we have to restrict the supremum to functions f that are orthogonal to the nullspace of $\mathcal{M}$.

Minimizing the maximum risk with respect to the mollifier kernel ψ, we end up with the minimax error

$$\inf_{\psi \in L^2([-1,1])} \sup_{\substack{f \in H^s(\mathbb{S}^2) \\ \|f\|_{H^s} \leq S}} \mathbb{E}\,\|f - \mathcal{E}_{N,\psi}(\mathcal{M}f + \varepsilon)\|_{L^2}^2 . \tag{3.3}$$

Looking at the minimax risk for such Sobolev balls is a standard approach in statistical inverse problems, cf. [4]. We aim at mollifiers for which the minimax risk is attained asymptotically as $N \to \infty$.

3.2 Lower Bounds

In this section, we aim at lower bounds for the minimax error (3.3). Since $\mathcal{E}_{N,\psi}$ is a linear estimator, the MISE it allows for the well known decomposition into a bias and a variance term

$$\|f - \mathcal{E}_{N,\psi}(\mathcal{M}f + \varepsilon)\|_{L^2}^2 = \|f - \psi \star \mathcal{M}^+\mathcal{L}_N\mathcal{M}f\|_{L^2}^2 + \mathbb{E}\,\|\psi \star \mathcal{M}^+\mathcal{L}_N\varepsilon\|_{L^2}^2 . \tag{3.4}$$

In a first step we bound the variance term $\mathbb{E}\,\|\psi \star \mathcal{M}^+\mathcal{L}_N\varepsilon\|_{L^2}^2$ by multiples of $\|\mathcal{M}^+\psi\|_{L^2}^2$ provided that the quadrature rule is exact for all polynomials up to a certain degree and that its weights are sufficiently uniform, cf. (2.8).

Theorem 3.2. *Let ψ be a polynomial of degree $N \in \mathbb{N}$ and let $Q_{\Xi,\Omega}$ be a spherical quadrature rule which is exact for polynomials of degree at most $2N$ and has positive weights $\omega_1, \ldots, \omega_M$ satisfying*

$$\delta_1 \frac{4\pi}{M} \leq \omega_m \leq \delta_2 \frac{4\pi}{M}, \quad m = 1, \ldots, M. \tag{3.5}$$

Furthermore, let ε be a white noise random field on the sphere with variance σ^2. Then the variance term in (3.4) satisfies

$$\delta_1 \frac{4\pi\sigma^2}{M} \|\mathcal{M}^+\psi\|_{L^2}^2 \leq \mathbb{E}\,\|\psi \star \mathcal{M}^+\mathcal{L}_N\varepsilon\|_{L^2}^2 \leq \delta_2 \frac{4\pi\sigma^2}{M} \|\mathcal{M}^+\psi\|_{L^2}^2 .$$

Proof. By Parseval's identity, the convolution formula (2.3) and the stochastic independence of the noise $\varepsilon_m = \varepsilon(\boldsymbol{\xi}_m)$, $m = 1, \dots, M$ we have

$$\begin{aligned}
\mathbb{E}\,\|\psi \star \mathcal{M}^+\mathcal{L}_N\varepsilon\|_{L^2}^2 &= \mathbb{E}\sum_{(n,k)\in I_N}\left|\hat{\mathcal{M}}^+(n)\right|^2|\hat{\psi}(n)|^2\left|\sum_{m=0}^{M}\varepsilon_m\omega_m\overline{Y_n^k(\boldsymbol{\xi}_m)}\right|^2 \\
&= \sum_{(n,k)\in I_N}\left|\hat{\mathcal{M}}^+(n)\right|^2|\hat{\psi}(n)|^2\sum_{m,m'=0}^{M}\omega_m\omega_{m'}\overline{Y_n^k(\boldsymbol{\xi}_m)}Y_n^k(\boldsymbol{\xi}_{m'})\mathbb{E}\varepsilon_m\overline{\varepsilon_{m'}} \\
&= \sigma^2\sum_{(n,k)\in I_N}\left|\hat{\mathcal{M}}^+(n)\right|^2|\hat{\psi}(n)|^2\sum_{m=0}^{M}\omega_m^2\left|Y_n^k(\boldsymbol{\xi}_m)\right|^2.
\end{aligned}$$

Next we make use of the estimate (3.5) and the fact that the quadrature rule is exact for polynomials of degree at most $2N$ and obtain

$$\begin{aligned}
\|\psi \star \mathcal{M}^+\mathcal{L}_N\,\varepsilon\|_{L^2}^2 &\le \delta_2\frac{4\pi\sigma^2}{M}\sum_{(n,k)\in I_N}|\hat{\mathcal{M}}^+(n)|^2\,|\hat{\psi}(n)|^2\sum_{m=0}^{M}\omega_m\left|Y_n^k(\boldsymbol{\xi}_m)\right|^2 \\
&= \delta_2\sigma^2\frac{4\pi}{M}\,\|\mathcal{M}^+\psi\|_{L^2}^2\,.
\end{aligned}$$

■

For the lower bound of the minimax error (3.3), we consider the following family of kernel functions with polynomially decreasing Legendre coefficients.

Definition 3.3. For $s, \tilde{N} > 0$ the mollifier $\psi_{\tilde{N}}^s \in \Pi_{\lfloor\tilde{N}\rfloor}[-1,1])$ is defined as

$$\psi_{\tilde{N}}^s = \sum_{n=0}^{\lfloor\tilde{N}\rfloor}\frac{2n+1}{4\pi}\left(1-\left(\frac{n+\frac{1}{2}}{\tilde{N}+\frac{1}{2}}\right)^s\right)P_n, \tag{3.6}$$

where $\lfloor\tilde{N}\rfloor$ is the largest integer not greater than $\tilde{N}$, see Figure 1.

With these mollifiers we obtain a lower bound of the MISE for any mollifier $\psi \in L^2([-1,1])$.

Lemma 3.4. *Let $N \in \mathbb{N}$, $s > 1$, $S > 0$, $\psi \in L^2([-1,1])$ be an arbitrary mollifier and let the quadrature Q be a quadrature formula which is exact for polynomials of degree at most $2N$. Then there is a polynomial degree $0 \le \tilde{N} \le N$, such that the mollifier $\psi_{\tilde{N}}^s$ gives the following lower bound of the maximum risk*

$$\sup_{\|f\|_{H^s}\le S}\mathbb{E}\,\|f - \mathcal{E}_{N,\psi}(\mathcal{M}f+\varepsilon)\|_{L^2}^2 \ge \frac{4\pi\sigma^2}{M}\delta_1\,\|\mathcal{M}^+\psi_{\tilde{N}}^s\|_{L^2}^2 + (\tilde{N}+\tfrac{1}{2})^{-2s}S^2.$$

Proof. Let $\tilde{N} > 0$ be the maximum value such that all Legendre coefficients of $\psi_{\tilde{N}}^s$ are smaller or equal to the Legendre coefficients of ψ, i.e.

$$\tilde{N} = \max\left\{N \ge 0 \mid \hat{\psi}_N^s(n) \le |\hat{\psi}(n)|\,,\ n \in \mathbb{N},\ \hat{\mathcal{M}}(n) \ne 0\right\}.$$

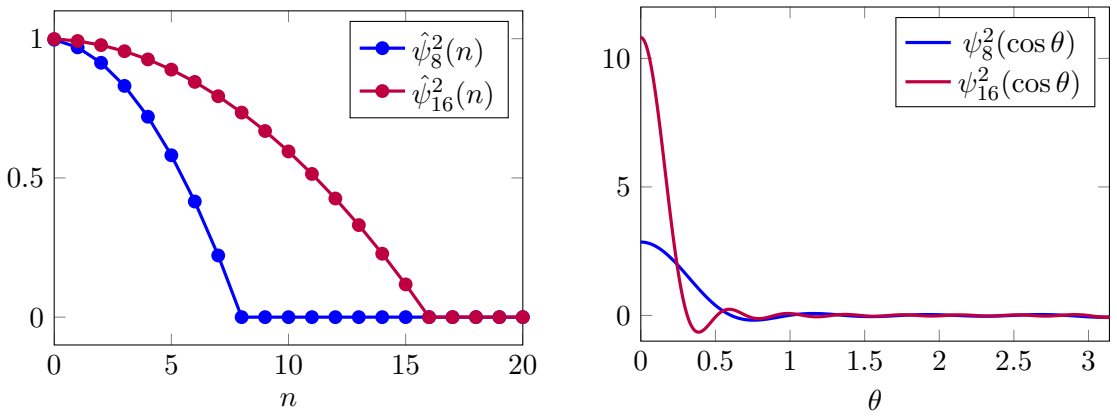

Figure 1: The mollifiers $\psi_{\tilde{N}}^s$ from Definition 3.3 are illustrated for $s = 2$ and $\tilde{N} \in \{8, 16\}$. The left image shows their Fourier coefficients, and the right one shows their function values depending on the polar angle θ.

Furthermore, we denote by $\tilde{n} \in \mathbb{N}$ the polynomial degree such that $\hat{\psi}_s^{\tilde{N}}(\tilde{n}) = |\hat{\psi}(\tilde{n})|$ and consider the function

$$\tilde{f}(\boldsymbol{\xi}) = \frac{S}{(\tilde{n} + \frac{1}{2})^s} Y_{\tilde{n},0}(\boldsymbol{\xi}), \quad \boldsymbol{\xi} \in \mathbb{S}^2.$$

Obviously, we have $\tilde{f} \in H^s(\mathbb{S}^2)$ and $\|\tilde{f}\|_{H^s} = S$. Since, $\tilde{f}$ is a spherical polynomial of degree $\tilde{n} \leq \tilde{N}$ so is $\mathcal{M}f$, and we have $\mathcal{M}^+\mathcal{L}_N\mathcal{M}\tilde{f} = \tilde{f}$. Hence, the bias term consists only of the smoothing error. The spherical convolution theorem (2.3) gives

$$\|\tilde{f} - \psi \star \mathcal{M}^+\mathcal{L}_N\mathcal{M}\tilde{f}\|_{L^2}^2 = \|\tilde{f} - \psi \star \tilde{f}\|_{L^2}^2 = \frac{|1 - \hat{\psi}(\tilde{n})|^2}{(\tilde{n} + \frac{1}{2})^{2s}} S^2 = \left(\tilde{N} + \frac{1}{2}\right)^{-2s} S^2.$$

Since by construction $\hat{\psi}_{\tilde{N}}^s(n) \leq |\hat{\psi}(n)|$ we conclude $\|\psi_{\tilde{N}}^s\|_{L^2} \leq \|\psi\|_{L^2}$. In conjunction with (3.4) and Theorem 3.2 we obtain

$$\begin{aligned}
\sup_{\|f\|_{H^s} \leq S} \mathbb{E}\,\|f - \mathcal{E}_{N,\psi}(\mathcal{M}f + \varepsilon)\|_{L^2}^2 &\geq \mathbb{E}\,\|\tilde{f} - \mathcal{E}_{N,\psi}(\mathcal{M}\tilde{f} + \varepsilon)\|_{L^2}^2 \\
&\geq \frac{4\pi\sigma^2}{M}\delta_1 \|\mathcal{M}^+\psi\|^2 + \|\tilde{f} - \psi \star \tilde{f}\|_{L^2}^2 \\
&\geq \frac{4\pi\sigma^2}{M}\delta_1 \|\mathcal{M}^+\psi_{\tilde{N}}\|_{L^2}^2 + \left(\tilde{N} + \frac{1}{2}\right)^{-2s} S^2.
\end{aligned}$$

■

In order to obtain exact constants, we have to evaluate $\|\mathcal{M}^+\psi_{\tilde{N}}^s\|_{L^2}$. In the following lemma, we do this for Fourier multiplication operators $\mathcal{M}$ whose symbols satisfy $\left|\hat{\mathcal{M}}(n)\right| \sim n^{-\beta}$ for $n \to \infty$.

Lemma 3.5. *For $s, \beta > 0$, let $\mathcal{M}\colon H^s \to H^{s+\beta}$ be a bounded and open Fourier multiplication operator, i.e, its symbol satisfies*

$$\|\mathcal{M}^+\|_{H^{s+\beta} \to H^s} (n + \tfrac{1}{2})^{-\beta} \leq \left|\hat{\mathcal{M}}(n)\right| \leq \|\mathcal{M}\|_{H^s \to H^{s+\beta}} (n + \tfrac{1}{2})^{-\beta}$$

for all $n \in \mathbb{N}$, and let

$$C_1 = \frac{s^2}{(\beta+1)(s+\beta+1)(s+2\beta+2)}. \tag{3.7}$$

Then we have

$$C_1 \left\|\mathcal{M}\right\|_{H^s \to H^{s+\beta}}^{-2} \tilde{N}^{2\beta+2} \leq \left\|\mathcal{M}^+ \psi_{\tilde{N}}^s\right\|_{L^2}^2 + o(\tilde{N}^{2\beta+2}) \leq C_1 \left\|\mathcal{M}^+\right\|_{H^{s+\beta} \to H^s}^2 \tilde{N}^{2\beta+2} \tag{3.8}$$

for $\tilde{N} \to \infty$.

Proof. The first inequality of (3.8) follows from

$$\begin{aligned}
\left\|\mathcal{M}^+ \psi_{\tilde{N}}^s\right\|_{L^2}^2 &= \sum_{n=0}^{\tilde{N}} (2n+1) \left|\hat{\mathcal{M}}^+(n)\right|^2 \left|\hat{\psi}(n)\right|^2 \\
&\leq 2 \left\|\mathcal{M}^+\right\|_{H^{s+\beta} \to H^s}^2 \sum_{n=0}^{\tilde{N}} (n+\tfrac{1}{2})^{2\beta+1} \left(1 - \left(\frac{n+\frac{1}{2}}{\tilde{N}+\frac{1}{2}}\right)^s\right)^2 \\
&\leq 2 \left\|\mathcal{M}^+\right\|_{H^{s+\beta} \to H^s}^2 \int_0^{\tilde{N}} n^{2\beta+1} \left(1 - \left(\frac{n}{\tilde{N}}\right)^s\right)^2 \mathrm{d}n + o(\tilde{N}^{2\beta+1}) \\
&= \frac{s^2 \left\|\mathcal{M}^+\right\|_{H^{s+\beta} \to H^s}^2}{(\beta+1)(s+\beta+1)(s+2\beta+2)} \tilde{N}^{2\beta+2} + o(\tilde{N}^{2\beta+1}).
\end{aligned}$$

The second inequality can be obtained analogously. ∎

Combining the last two lemmas, we obtain a lower bound for the minimax risk.

Theorem 3.6. *Let $s > 1$, $S, \beta > 0$ and $\mathcal{M} \colon H^s(\mathbb{S}^2) \to H^{s+\beta}(\mathbb{S}^2)$ be a bounded and open Fourier multiplication operator. Let, furthermore, $Q_{\Xi,\Omega}$ be a quadrature rule that is exact for polynomials of degree at most $2N$ and consists of M points. Then the minimax risk for Sobolev balls in $H^s(\mathbb{S}^2)$ and the family of estimators $\mathcal{E}_{N,\psi}$, $\psi \in L^2([-1,1])$ is bounded from below by*

$$\inf_{\psi \in L^2([-1,1])} \sup_{\|f\|_{H^s} \leq S} \mathbb{E} \left\|f - \mathcal{E}_{N,\psi}(\mathcal{M}f + \varepsilon)\right\|_{L^2}^2 \geq C_2 \left(\frac{4\pi\sigma^2\delta_1 C_1}{\left\|\mathcal{M}\right\|_{H^s \to H^{s+\beta}}^2}\right)^{\frac{s}{s+\beta+1}} S^{\frac{2\beta+2}{s+\beta+1}} M^{-\frac{s}{s+\beta+1}}, \tag{3.9}$$

where

$$C_2 = \left(\frac{s}{\beta+1}\right)^{\frac{\beta+1}{s+\beta+1}} + \left(\frac{\beta+1}{s}\right)^{\frac{s}{s+\beta+1}}.$$

Proof. Combining Lemma 3.4 and Lemma 3.5 we have for any function $\psi \in L^2([-1,1])$,

$$\begin{aligned}
\sup_{\|f\|_{H^s} \leq S} \mathbb{E} \left\|f - \mathcal{E}_{N,\psi}(\mathcal{M}f + \varepsilon)\right\|_{L^2}^2 &\geq \inf_{0 \leq \tilde{N} \leq N} \frac{4\pi\sigma^2}{M} \delta_1 \left\|\mathcal{M}^+ \psi_{\tilde{N}}^s\right\|_{L^2}^2 + (\tilde{N}+\tfrac{1}{2})^{-2s} S^2 \\
&\approx \inf_{0 \leq \tilde{N} \leq N} \frac{4\pi\sigma^2\delta_1 C_1}{M \left\|\mathcal{M}\right\|_{H^s \to H^{s+\beta}}^2} \tilde{N}^{2\beta+2} + \tilde{N}^{-2s} S^2.
\end{aligned}$$

where we have ignored lower order terms of $\tilde{N}$. Minimizing the last term with respect to $\tilde{N}$ we obtain

$$\tilde{N}^{2s+2\beta+2} = \frac{2sS^2 M \left\|\mathcal{M}\right\|_{H^s \to H^{s+\beta}}^2}{4\pi\sigma^2\delta_1 C_1 (2\beta+2)} \tag{3.10}$$

and

$$\sup_{\|f\|_{H^s}\leq S} \mathbb{E}\,\|f-\mathcal{E}_{N,\psi}(\mathcal{M}f+\varepsilon)\|_{L^2}^2 \geq C_2\left(\frac{4\pi\sigma^2\delta_1 C_1}{\|\mathcal{M}\|_{H^s\to H^{s+\beta}}^2}\right)^{\frac{2s}{2s+2\beta+2}} S^{\frac{4\beta+4}{2s+2\beta+2}} M^{-\frac{2s}{2s+2\beta+2}}$$

with C_2 as in (3.6). Since $M\sim N^2$, we have $\tilde{N}<N$ for sufficiently large N. ■

3.3 Upper Bounds

Having found lower bounds for the minimax risk using the family of mollifiers ψ_N^s, we aim at upper bounds using the same mollifiers and show that upper and lower bounds have the same asymptotic rate with respect to the number of sampling points.

Our upper bound is based on splitting the bias error

$$\|f-\psi\star\mathcal{M}^+\mathcal{L}_N\mathcal{M}f\|_{L^2} \leq \|f-\psi\star f\|_{L^2} + \|\psi\star(f-\mathcal{M}^+\mathcal{L}_N\mathcal{M}f)\|_{L^2} \tag{3.11}$$

into a smoothing error $\|f-\psi\star f\|_{L^2}$ and an aliasing error $\|\psi\star(f-\mathcal{M}^+\mathcal{L}_N\mathcal{M}f)\|_{L^2}$. For the smoothing error we have the following upper bound.

Lemma 3.7. *Let $\psi\in L^2([-1,1])$. Provided that $f\in H^s(\mathbb{S}^2)$ for some $s>0$, the smoothing error is bounded by*

$$\|f-\psi\star f\|_{L^2} \leq \|f\|_{H^s}\sup_{n\in\mathbb{N}}\frac{|1-\hat{\psi}(n)|}{(n+\frac{1}{2})^s}.$$

For the mollifier $\psi_{\tilde{N}}^s$ as defined in (3.6)*, the upper bound becomes*

$$\|f-\psi_{\tilde{N}}^s\star f\| \leq \|f\|_{H^s}\,(\tilde{N}+\tfrac{1}{2})^{-s}$$

Proof. This lemma is a direct consequence of Parseval's identity and the convolution formula (2.3). ■

For the aliasing error we obtain the following bound.

Lemma 3.8. *Let $\mathcal{M}\colon H^s(\mathbb{S}^2)\to H^{s+\beta}$ be a bounded Fourier multiplication operator, $s>1$ and $f\in\mathcal{M}^+H^{s+\beta}(\mathbb{S}^2)$. Then for any mollifier $\psi\in L^2([-1,1])$ that satisfies $\hat{\psi}(n)\in[0,1]$ for all $n\in\mathbb{N}$, the aliasing error is bounded by*

$$\|\psi\star(f-\mathcal{M}^+\mathcal{L}_N\mathcal{M}f)\|_{L^2} \leq C_3(N+\tfrac{1}{2})^{1-s}\,\|\mathcal{M}^+\|_{H^{s+\beta}\to H^s}\,\|\mathcal{M}\|_{H^s\to H^{s+\beta}}\,\|f\|_{H^s},$$

where the constant C_3 is independent of N and f.

Proof. By Theorem 2.4 we have

$$\begin{aligned}\|\psi\star(f-\mathcal{M}^+\mathcal{L}_N\mathcal{M}f)\|_{L^2} &\leq \|\mathcal{M}^+\mathcal{M}f-\mathcal{M}^+\mathcal{L}_N\mathcal{M}f\|_{L^2} \leq \|\mathcal{M}^+\|_{H^{s+\beta}\to H^s}\,\|\mathcal{M}f-\mathcal{L}_N\mathcal{M}f\|_{L^2}\\ &\leq C\,(N+\tfrac{1}{2})^{1-s}\,\|\mathcal{M}^+\|_{H^{s+\beta}\to H^s}\,\|\mathcal{M}\|\,\|f\|_{H^s}.\end{aligned}$$

■

Combining Lemma 3.7, 3.8 and 3.5 with the optimal parameter $\tilde{N}$ found in Theorem 3.6, eq. (3.10), we end up with the following upper bound for the MISE.

Theorem 3.9. *For some $\beta > 0$, $s > \frac{1-\beta}{2} + \frac{1}{2}\sqrt{\beta^2+2\beta+5}$, $S > 0$ and $\sigma > 0$, let $\mathcal{M}\colon H^s(\mathbb{S}^2) \to H^{s+\beta}$ be a bounded Fourier multiplication operator. Assume, further, that the quadrature rule $Q_{N,\Xi}$ is exact for spherical polynomials of degree $2N$ and consists of $|\Xi| = M \sim N^2$ quadrature points. Then an asymptotic upper bound for the minimax risk of the estimator $\mathcal{E}_{N,\psi} g = \psi \star \mathcal{M}^+ \mathcal{L}_N g$ is given by*

$$\inf_{\psi \in L^2([-1,1])} \sup_{\substack{f \in H^s(\mathbb{S}^2) \\ \|f\|_{H^s} \le S}} \mathbb{E}\, \|f - \mathcal{E}_{N,\psi}(\mathcal{M}f + \varepsilon)\|_{L^2}^2 \le C_2 \left(4\pi\sigma^2\delta_2 C_1 \|\mathcal{M}^+\|_{H^{s+\beta}\to H^s}^2\right)^{\frac{s}{s+\beta+1}} S^{\frac{2\beta+2}{s+\beta+1}} M^{-\frac{s}{s+\beta+1}},$$

with the constants C_1 and C_2 as defined in Theorem 3.6.

Proof. By the decomposition of the MISE (3.11) in combination with Lemma 3.7 and 3.8, we have for any $0 \le \tilde{N} \le N$

$$\begin{aligned}
&\inf_{\psi \in L^2([-1,1])} \sup_{\substack{f \in H^s(\mathbb{S}^2) \\ \|f\|_{H^s} \le S}} \mathbb{E}\, \|f - \mathcal{E}_{N,\psi}(\mathcal{M}f + \varepsilon)\|_{L^2}^2 \\
&\quad \le \sup_{\substack{f \in H^s(\mathbb{S}^2) \\ \|f\|_{H^s} \le S}} \mathbb{E}\, \|f - \mathcal{E}_{N,\psi^s_{\tilde{N}}}(\mathcal{M}f + \varepsilon)\|_{L^2}^2 \\
&\quad \le \left(\|f - \psi^s_{\tilde{N}} \star f\|_{L^2} + \|\psi^s_{\tilde{N}} \star (f - \mathcal{M}^+\mathcal{L}_N\mathcal{M}f)\|_{L^2}\right)^2 + \frac{4\pi\sigma^2\delta_2}{M} \|\mathcal{M}^+\psi^s_{\tilde{N}}\|_{L^2}^2 \\
&\quad \le \left((\tilde{N}+\tfrac{1}{2})^{-s} + \tilde{C}_3\left(N+\tfrac{1}{2}\right)^{1-s}\right)^2 S^2 + \frac{4\pi\sigma^2\delta_2 C_1 \|\mathcal{M}^+\|_{H^{s+\beta}\to H^s}^2}{M} \tilde{N}^{2\beta+2}. \quad (3.12)
\end{aligned}$$

where C_1 is the constant defined in Lemma 3.5 and $\tilde{C}_3 = C_3 \|\mathcal{M}\|_{H^s\to H^{s+\beta}} \|\mathcal{M}^+\|_{H^{s+\beta}\to H^s}$ is defined upon Lemma 3.8.

Recall from the proof of Theorem 3.6, eq. (3.10), that the sum $\tilde{N}^{-2s} + M^{-1}\tilde{N}^{2\beta+2}$ is minimal for $\tilde{N} \sim M^{\frac{1}{2s+2\beta+2}}$. With the assumption $N \sim M^{1/2} \sim \tilde{N}^{s+\beta+1}$, we observe that, when we suppress all constants, the right side of (3.12) becomes

$$\left(\tilde{N}^{-s} + \tilde{N}^{(1-s)(s+\beta+1)}\right)^2 + \tilde{N}^{-2s}.$$

Thus the aliasing error $\tilde{N}^{(1-s)(s+\beta+1)}$ is asymptotically negligible compared to the smoothing error $\tilde{N}^{-2s}$ for $M \to \infty$, whenever $(1-s)(s+\beta+1) < -s$, which is equivalent to the condition on s. Within this setting, minimizing the smoothing error and the variance term with respect to $\tilde{N}$ we obtain analogously to (3.10) in Theorem 3.6

$$\tilde{N}^{2s+2\beta+2} = \frac{sS^2M}{4\pi\sigma^2\delta_2 C_1(\beta+1)\|\mathcal{M}^+\|_{H^{s+\beta}\to H^s}^2}$$

and

$$\begin{aligned}
&\inf_{0 \le \tilde{N} \le N} \sup_{\substack{f \in H^s(\mathbb{S}^2) \\ \|f\|_{H^s} \le S}} \mathbb{E}\, \|f - \mathcal{E}_{N,\psi^s_{\tilde{N}}}(\mathcal{M}f + \varepsilon)\|_{L^2}^2 \\
&\le C_2 \left(4\pi\sigma^2\delta_2 C_1 \|\mathcal{M}^+\|_{H^{s+\beta}\to H^s}^2\right)^{\frac{s}{s+\beta+1}} S^{\frac{2\beta+2}{s+\beta+1}} M^{-\frac{s}{s+\beta+1}},
\end{aligned} \quad (3.13)$$

with C_2 as defined in Theorem 3.6. ∎

3.4 Asymptotically sharp bounds

In the previous two sections, we have derived lower and upper bounds of the minimax error. These two bounds from (3.9) and (3.13) only differ in two points, namely the constants δ_1 and δ_2 of the quadrature as well as the norms of $\mathcal{M}$ and its inverse. Now we take a look at a situation in which these two bounds become sharp.

Theorem 3.10. *Let the conditions from Theorem 3.9 hold. Assume, further, that the hyperinterpolation operator $\mathcal{L}_N$ is based on a spherical $2N$-design that has cardinality $M \sim N^2$ and the symbol of the Fourier multiplication operator $\mathcal{M} : H^s(\mathbb{S}^2) \to H^{s+\beta}(\mathbb{S}^2)$ satisfies*

$$\lim_{n\to\infty} \left(n + \frac{1}{2}\right)^{\beta} \left|\hat{\mathcal{M}}(n)\right| = \alpha > 0. \tag{3.14}$$

Then the lower and upper bound of the asymptotic minimax error from Theorems 3.6 and 3.9, respectively, coincide for the regularization parameter

$$\tilde{N}^* = \left(\frac{sS^2M\alpha^2}{4\pi\sigma^2 C_1(\beta+1)}\right)^{\frac{1}{2s+2\beta+2}}, \tag{3.15}$$

and thus we have the minimax error

$$\inf_{\psi\in L^2([-1,1])} \sup_{\substack{f\in H^s(\mathbb{S}^2)\\ \|f\|_{H^s}\le S}} \mathbb{E}\,\|f - \mathcal{E}_{N,\psi}(\mathcal{M}f+\varepsilon)\|_{L^2}^2 \simeq \sup_{\substack{f\in H^s(\mathbb{S}^2)\\ \|f\|_{H^s}\le S}} \mathbb{E}\,\|f - \mathcal{E}_{N,\psi^s_{\tilde{N}^*}}(\mathcal{M}f+\varepsilon)\|_{L^2}^2$$

for $M \to \infty$, where "$\simeq$" means that the limit of the quotient of the two terms equals one.

Proof. This follows from the proofs of Theorems 3.6 and 3.9. Firstly, we see that $\delta_1 = \delta_2$ due to the spherical designs. Secondly, we can replace $\|\mathcal{M}\|_{H^s\to H^{s+\beta}}$ and $\|\mathcal{M}^+\|^{-1}_{H^{s+\beta}\to H^s}$ with α for the respective bounds of the symbol $\left|\hat{\mathcal{M}}(n)\right|$ for $n \to \infty$. Therefore, the lower and upper bounds (3.9) and (3.13) coincide. ∎

The first condition of this theorem, to use a spherical design, is quite some restriction on the quadrature rule, but such spherical designs are known to exist and can be computed numerically up to a certain degree, see Section 2.3. The second one, that the limit in (3.14) exists, is a little more natural. If $\mathcal{M}$ is an open operator, we already have by (2.4) that the term $\left(n+\frac{1}{2}\right)^{\beta}\left|\hat{\mathcal{M}}(n)\right|$ is bounded away from zero.

Theorem 3.10 gives an asymptotically exact expression of the minimax error. The minimax error is asymptotically achieved with the mollifier $\psi^s_{\tilde{N}^*}$. Therefore, the family of mollifiers $\psi^s_{\tilde{N}}$ from Definition 3.3 is asymptotically optimal, so we do not have to minimize the MISE over all mollifiers $\psi \in L^2([-1,1])$. Instead, it suffices to look at those mollifiers from this family and we can be sure that we still asymptotically achieve the minimax error. This fact also comes in handy in practical situations. Since the Sobolev norm of the solution f is usually unknown, we cannot compute $\tilde{N}^*$ as in (3.15). However, there are various methods described in literature to choose the parameter $\tilde{N}$ in order to minimize the error, cf. [1].

Application to the Funk–Radon and cosine transform. We want to apply our previous results to the Funk–Radon transform $\mathcal{F}$ and the cosine transform $\mathcal{C}$, which were defined in (1.1) and (1.3), respectively. Even though these two transforms are Fourier multiplication operators by Lemma 2.2, we cannot use Theorem 3.10 immediately, because these two transforms have nonempty nullspaces consisting of all odd functions. So it makes sense to reconstruct only even functions. We denote by $L^2_{\mathrm{e}}(\mathbb{S}^2)$ and $H^s_{\mathrm{e}}(\mathbb{S}^2)$ the respective subspaces of the Lebesgue space $L^2(\mathbb{S}^2)$ and the Sobolev space $H^s(\mathbb{S}^2)$ that contain only the even functions, i.e. $f(\boldsymbol{\xi}) = f(-\boldsymbol{\xi})$ for all $\boldsymbol{\xi} \in \mathbb{S}^2$.

To reconstruct even functions, we assume the mollifiers ψ to be even functions, too, i.e. $\psi(t) = \psi(-t)$ for all $t \in [-1, 1]$. As mollifiers we can take the even parts of those from Definition 3.3. For $\tilde{N} > 0$, we define

$$\psi^{s,\mathrm{e}}_{\tilde{N}} = \sum_{n=0}^{\lfloor \tilde{N}/2 \rfloor} (4n+1) \left(1 - \left(\frac{2n+\frac{1}{2}}{\tilde{N}+\frac{1}{2}}\right)^s\right) P_{2n}. \tag{3.16}$$

Lemma 2.2 implies formulas similar to (3.14) for the Funk–Radon and cosine transform, namely

$$\lim_{n\to\infty} \left|\hat{\mathcal{F}}(2n)\right| \cdot \left(2n+\frac{1}{2}\right)^{1/2} = \sqrt{\frac{2}{\pi}}$$

and

$$\lim_{n\to\infty} \left|\hat{\mathcal{C}}(2n)\right| \cdot \left(2n+\frac{1}{2}\right)^{5/2} = 4\sqrt{2\pi},$$

respectively. Now we look at what happens to our computations in Sections 3.2 and 3.3 if the mollifier ψ is assumed to be an even function. In Lemma 3.5, it is easy to see that the norm of the even mollifier is just the half of that from (3.8). Thus, the constant C_1 is now half of the value from (3.7) in this situation. The rest of these sections remains the same as before with the only exception of C_1. So we replace C_1 by $\frac{C_1}{2}$ whenever it appears. The following corollary is a rewritten version of Theorem 3.10 adapted to the Funk–Radon and the spherical cosine transform.

Corollary 3.11. We denote by $\mathcal{M}$ either the Funk–Radon transform or the spherical cosine transform. Let $s > s^{\min}_{\mathcal{M}}$, $S > 0$ and $\sigma > 0$, where $s^{\min}_{\mathcal{F}} = \frac{3}{2}$ and $s^{\min}_{\mathcal{C}} = -\frac{3}{4} + \frac{\sqrt{65}}{4}$. For every $N \in \mathbb{N}$, let $\mathcal{L}_N$ be a hyperinterpolation operator on the sphere that is based on a spherical $2N$-design with $M \sim N^2$ nodes, cf. Section 2.3. Then the minimax risk for Sobolev balls of radius S in $H^s_{\mathrm{e}}(\mathbb{S}^2)$ and the family of estimators $\mathcal{E}_{N,\psi}$, $\psi \in L^2_{\mathrm{e}}([-1,1])$, for the inversion of the Funk–Radon or spherical cosine transform is asymptotically for $N \to \infty$ achieved by the mollifiers $\psi^{s,\mathrm{e}}_{\tilde{N}^*_{\mathcal{M}}}$ from (3.16) with the parameters

$$\tilde{N}^*_{\mathcal{F}} = \frac{S^2 M (3+s)(\frac{3}{2}+s)}{\pi^2 \sigma^2 s} \quad \text{or} \quad \tilde{N}^*_{\mathcal{C}} = \frac{16 S^2 M (7+s)(\frac{7}{2}+s)}{\sigma^2 s}, \tag{3.17}$$

respectively. Furthermore, we have the asymptotic minimax error for $M \to \infty$

$$\inf_{\psi \in L^2_{\mathrm{e}}([-1,1])} \sup_{\substack{f \in H^s_{\mathrm{e}}(\mathbb{S}^2) \\ \|f\|_{H^s} \le S}} \mathbb{E}\, \|f - \mathcal{E}_{N,\psi}(\mathcal{M}f + \varepsilon)\|^2_{L^2} \simeq \sup_{\substack{f \in H^s_{\mathrm{e}}(\mathbb{S}^2) \\ \|f\|_{H^s} \le S}} \mathbb{E}\, \|f - \mathcal{E}_{N,\psi^s_{\tilde{N}^*_{\mathcal{M}}}}(\mathcal{M}f + \varepsilon)\|^2_{L^2}.$$

For the Funk–Radon transform $\mathcal{M} = \mathcal{F}$, the minimax error is asymptotically equal to

$$\left(\left(\frac{2s}{3}\right)^{\frac{3}{2s+3}} + \left(\frac{3}{2s}\right)^{\frac{2s}{2s+3}}\right)\left(\frac{2\pi^2\sigma^2 s^2}{3\left(s+\frac{3}{2}\right)(s+3)}\right)^{\frac{2s}{2s+7}} S^{\frac{3}{2s+3}} M^{-\frac{2s}{2s+3}}, \tag{3.18}$$

and for the cosine transform $\mathcal{M} = \mathcal{C}$, the minimax error reads

$$\left(\left(\frac{2s}{7}\right)^{\frac{7}{2s+7}} + \left(\frac{7}{2s}\right)^{\frac{2s}{2s+7}}\right)\left(\frac{\sigma^2 s^2}{56\left(s+\frac{7}{2}\right)(s+7)}\right)^{\frac{2s}{2s+7}} S^{\frac{7}{2s+7}} M^{-\frac{2s}{2s+7}}. \tag{3.19}$$

4 Numerical Experiments

In this section we give fast algorithms for the forward transform $\mathcal{M}$ as well as for the inverse transform, i.e., for the computation of the estimator $\mathcal{E}_{N,\psi}(\mathcal{M}f + \varepsilon)$. Those algorithms will be applied to illustrate the numerical findings of the previous sections, i.e. the asymptotic decay of the MISE as well as the optimality of the mollifiers defined in Definition 3.3.

4.1 Fast algorithms for the direct and the inverse transform

The forward transform. Let $\mathcal{M}$ be a Fourier multiplication operator and $f \in L^2(\mathbb{S}^2)$ such that $\mathcal{M}f\colon \mathbb{S}^2 \to \mathbb{C}$ is a continous function. Then

$$\mathcal{M}f(\boldsymbol{\eta}) = \sum_{(n,k)\in I} \hat{\mathcal{M}}(n)\left(\int_{\mathbb{S}^2} f(\boldsymbol{\xi})\overline{Y_n^k(\boldsymbol{\xi})}\,\mathrm{d}\boldsymbol{\xi}\right) Y_n^k(\boldsymbol{\eta}), \quad \boldsymbol{\eta}\in\mathbb{S}^2. \tag{4.1}$$

In order to compute this formula numerically, we make two modifications. Firstly, the sum is truncated at a certain degree $N \in \mathbb{N}$. Secondly, the integral over the sphere is replaced by a quadrature rule with nodes $\boldsymbol{\xi}_m \in \mathbb{S}^2$ and weights ω_m, $m = 1,\dots,M$. Let $\mathcal{L}_N$ be the corresponding hyperinterpolation operator on the sphere, cf. Section 2.3. The modifications yield

$$\mathcal{M}\mathcal{L}_N f(\boldsymbol{\eta}) = \sum_{(n,k)\in I_N} \hat{\mathcal{M}}(n)\left(\sum_{m=1}^{M} \omega_m f(\boldsymbol{\xi}_m)\overline{Y_n^k(\boldsymbol{\xi}_m)}\right) Y_n^k(\boldsymbol{\eta}), \quad \boldsymbol{\eta}\in\mathbb{S}^2. \tag{4.2}$$

In order evaluate $\mathcal{M}\mathcal{L}_N f$ at points $\boldsymbol{\eta}_j \in \mathbb{S}^2$, $j = 1,\dots,J$, we decompose the computation of (4.2) into a three-step process:

i) Compute

$$\widehat{\mathcal{L}_N f}(n,k) = \sum_{m=1}^{M} \omega_m f(\boldsymbol{\xi}_m)\overline{Y_n^k(\boldsymbol{\xi}_m)}, \quad (n,k)\in I_N.$$

ii) Multiply

$$[\mathcal{M}\mathcal{L}_N f]^\wedge(n,k) = \hat{\mathcal{M}}(n)\widehat{\mathcal{L}_N f}(n,k), \quad (n,k)\in I_N.$$

iii) Compute

$$\mathcal{M}\mathcal{L}_N f(\boldsymbol{\eta}_j) = \sum_{(n,k)\in I_N} [\mathcal{M}\mathcal{L}_N f]^\wedge(n,k) Y_n^k(\boldsymbol{\eta}_j), \quad j = 1,\dots,J.$$

If the hyperinterpolation $\mathcal{L}_N$ is exact the above algorithm is exact for polynomials up to degree N. In order to analyze the arithmetic complexity of the algorithm, we examine the three steps separately and assume that the number M of quadrature nodes and the number J of evaluation points are proportional to the dimension of the space of spherical polynomials of degree N, i.e., $J, M \in \mathcal{O}(N^2)$, which holds for sufficiently good quadrature rules, cf. Section 2.3. The third step is essentially a spherical Fourier transform while the first step is an adjoint spherical Fourier transform. Computing these transforms directly would need $\mathcal{O}(N^4)$ operations. Fortunately, there is a fast approximative algorithm known as the nonequispaced fast spherical Fourier transform (NFSFT) which has the numerical complexity $\mathcal{O}(N^2 \log^2 N)$, see [21] for the NFSFT and [17] for the adjoint NFSFT. These algorithms are available as part of the open source NFFT software library [20]. Since the second step of our algorithm consists of $\mathcal{O}(N^2)$ multiplications in Fourier space, the overall complexity is $\mathcal{O}(N^2 \log^2 N)$.

This algorithm is considerably faster than the direct computation of $\mathcal{M}f$ via quadrature: Suppose that $\mathcal{M}_h$ is a convolution operator with some function $h : [-1, 1] \to \mathbb{C}$ and we want to compute $\mathcal{M}_h f = h \star f$ at M points $\boldsymbol{\eta}_j \in \mathbb{S}^2$ by a quadrature rule. Then we have

$$\mathcal{M}_h f(\boldsymbol{\eta}_j) = \int_{\mathbb{S}^2} h(\boldsymbol{\xi} \cdot \boldsymbol{\eta}_j) f(\boldsymbol{\xi}) \mathrm{d}\boldsymbol{\xi} \approx \sum_{m=0}^{M} \omega_m h(\boldsymbol{\xi}_m \cdot \boldsymbol{\eta}_j) f(\boldsymbol{\xi}_m), \quad j = 1, \dots, M,$$

which requires $\mathcal{O}(M^2) = \mathcal{O}(N^4)$ numerical operations.

The inverse transform. Starting point for an algorithm implementing the inverse transform is the Fourier space representation of the estimator $\mathcal{E}_{N,\psi} g$,

$$\mathcal{E}_{N,\psi} g(\boldsymbol{\eta}) = \psi \star \mathcal{M}^+ \mathcal{L}_N \, g(\boldsymbol{\eta}) = \sum_{n=0}^{N} \hat{\mathcal{M}}^+(n) \hat{\psi}(n) \sum_{k=-n}^{n} \left(\sum_{m=1}^{M} \omega_m g(\boldsymbol{\xi}_m) \overline{Y_n^k(\boldsymbol{\xi}_m)} \right) Y_n^k(\boldsymbol{\eta}),$$

where $\mathcal{L}_N$ is the hyperinterpolation operator with respect to a quadrature rule with nodes $\boldsymbol{\xi}_m \in \mathbb{S}^2$ and weights ω_m, $m = 1, \dots, M$. The computation of function values $\mathcal{E}_{N,\psi} g(\boldsymbol{\eta}_j)$ at points $\boldsymbol{\eta}_j \in \mathbb{S}^2$, $j = 1, \dots, J$ given point evaluations $g(\boldsymbol{\xi}_m)$, $m = 1, \dots, M$ can be decomposed into the following three steps:

i) Compute the adjoint spherical Fourier transform

$$\widehat{\mathcal{L}_N g}(n, k) = \sum_{m=1}^{M} \omega_m g(\boldsymbol{\xi}_m) \overline{Y_n^k(\boldsymbol{\xi}_m)}, \quad (n, k) \in I_N.$$

ii) Multiply

$$\widehat{\mathcal{E}_{N,\psi} g}(n, k) = \hat{\psi}(n) \hat{\mathcal{M}}^+(n) \widehat{\mathcal{L}_N g}(n, k), \quad (n, k) \in I_N.$$

iii) Compute the spherical Fourier transform

$$\mathcal{E}_{N,\psi} g(\boldsymbol{\eta}_j) = \sum_{(n,k) \in I_N} \widehat{\mathcal{E}_{N,\psi} g}(n, k) Y_n^k(\boldsymbol{\eta}_j), \quad j = 1, \dots, J.$$

Analogously to the forward algorithm, the algorithm for the inverse transform consists of one spherical Fourier transform in step iii), one adjoint spherical Fourier transform in step i) and $\mathcal{O}(N^2)$ multiplications in Fourier space in step ii). Hence, the arithmetic complexity of this algorithm is again $\mathcal{O}(N^2 \log^2 N)$ operations provided that the NFSFT is used.

4.2 Some test function

As a test function we consider a linear combination of radial splines. The following lemma gives an explicit formula for the Funk–Radon transform of radial splines of order two.

Lemma 4.1. *For $h \in (0,1)$ and $\boldsymbol{\zeta} \in \mathbb{S}^2$, we define the radially symmetric and even function $f_h = \widetilde{f}_h(\circ \cdot \boldsymbol{\zeta}) \in C(\mathbb{S}^2)$ by*

$$\widetilde{f}_h(z) = (|z| - h)^2 \mathbf{1}_{[h,1]}(|z|), \quad z \in [-1,1], \tag{4.3}$$

where $\mathbf{1}_{[h,1]}$ denotes the indicator function of the interval $[h,1]$. Then f_h is continuously differentiable and its Funk–Radon transform $\mathcal{F}f_h = \widetilde{g}_h(\circ \cdot \boldsymbol{\zeta})$ is given by

$$\widetilde{g}_h(z) = \begin{cases} \frac{1}{\pi}\left(-3h\sqrt{1-z^2-h^2} + \left(1-z^2+2h^2\right)\arccos\frac{h}{\sqrt{1-z^2}}\right) & : |z| < \sqrt{1-h^2} \\ 0 & : \text{orherwise.} \end{cases}$$

Proof. Let $f = \tilde{f}(\circ \cdot \boldsymbol{e}_3) \in C\left(\mathbb{S}^2\right)$ be some arbitrary radially symmetric function with respect to the north pole $\boldsymbol{e}_3$ of the sphere. Then we have for its Funk–Radon transform

$$\mathcal{F}f(\boldsymbol{\xi}) = \frac{1}{2\pi}\int_{\boldsymbol{\eta}\cdot\boldsymbol{\xi}=0} \widetilde{f}(\boldsymbol{\eta}\cdot\boldsymbol{e}_3)\,\mathrm{d}\boldsymbol{\eta} = \frac{1}{2\pi}\int_{\boldsymbol{\eta}\cdot\boldsymbol{e}_3=0} \widetilde{f}(\boldsymbol{\eta}\cdot\boldsymbol{\xi})\,\mathrm{d}\boldsymbol{\eta}.$$

Writing the vectors $\boldsymbol{\xi}(\theta,\rho)$ and $\boldsymbol{\eta}\left(\frac{\pi}{2},\varphi\right)$, $\varphi \in [0,2\pi]$, in spherical coordinates, we have $\boldsymbol{\xi}\cdot\boldsymbol{\eta} = \sin(\theta)\cos(\rho-\varphi)$ and, therefore,

$$\mathcal{F}f(\boldsymbol{\xi}(\theta,\rho)) = \frac{1}{2\pi}\int_0^{2\pi} \widetilde{f}(\sin(\theta)\cos(\rho-\varphi))\,\mathrm{d}\varphi = \frac{1}{2\pi}\int_0^{2\pi} \widetilde{f}\left(\sqrt{1-(\boldsymbol{\xi}\cdot\boldsymbol{e}_3)^2}\cos(\varphi)\right)\mathrm{d}\varphi. \tag{4.4}$$

The above formula generalizes to radial function $f = \tilde{f}(\circ\cdot\boldsymbol{\zeta}) \in C\left(\mathbb{S}^2\right)$ with arbitrary symmetry axis. In particular, the Funk–Radon transform $\mathcal{F}f$ of a radial function is again a radial function.

Equation (4.4) applied to the even function f_h yields

$$\widetilde{g}_h(z) = \frac{1}{2\pi}\int_{-\pi}^{\pi}\left(\left|\sqrt{1-z^2}\cos(\varphi)\right| - h\right)^2 \mathbf{1}_{[h,1]}\left(\left|\sqrt{1-z^2}\cos(\varphi)\right|\right)\mathrm{d}\varphi,$$

where we have used that f_h is even. We see that $\widetilde{g}_h(z)$ vanishes for $\sqrt{1-z^2} < h$. Otherwise, we compute

$$\widetilde{g}_h(z) = \frac{1}{\pi}\left(-3h\sqrt{1-z^2-h^2} + \left(1-z^2+2h^2\right)\arccos\frac{h}{\sqrt{1-z^2}}\right).$$

It remains to show that f_h has a continuous derivative. As before, we assume, without loss of generality, $\boldsymbol{\zeta} = \boldsymbol{e}_3$ and observe that the derivative of $f_h(\boldsymbol{\xi}(\theta,\rho))$ with respect to the azimuth ρ vanishes for every $\boldsymbol{\xi} \in \mathbb{S}^2 \setminus \{\pm\boldsymbol{e}_3\}$. With respect to the polar angle θ, we have

$$\frac{\partial}{\partial\theta} f_h(\boldsymbol{\xi}(\theta,\rho)) = \frac{\partial}{\partial\theta}(\cos\theta - h)^2 = -2(\cos\theta - h)\sin(\theta)$$

for $\theta \in (0, \arccos h)$ and $\frac{\partial}{\partial\theta} f_h(\boldsymbol{\xi}(\theta,\rho)) = 0$ otherwise. In particular, the derivative of f_h vanishes at the north pole $\theta = 0$ and south pole $\theta = \pi$, which shows the continuity of the derivative. ∎

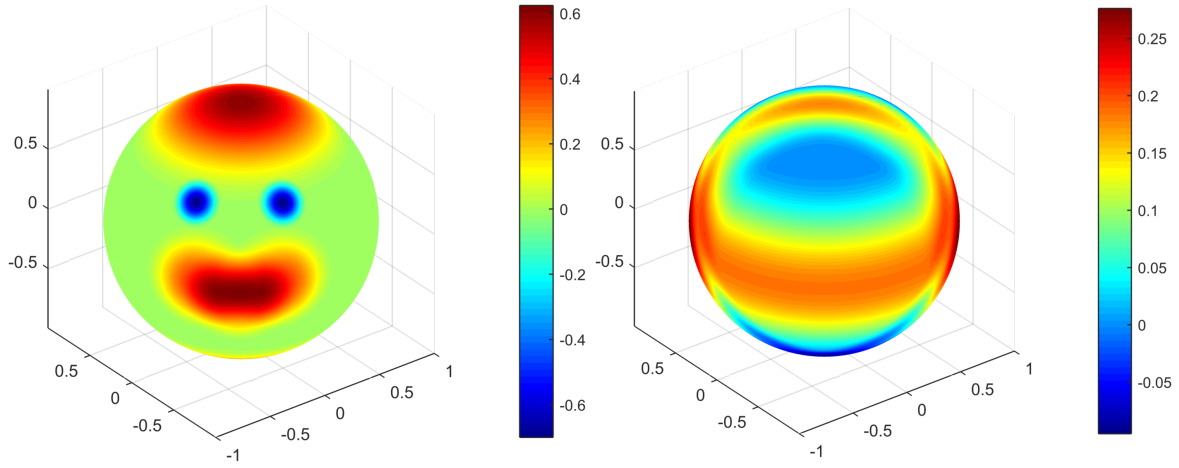

(a) The test function f

(b) Funk–Radon transform $\mathcal{F}f$ of the test function

Figure 2: The test function f is a weighted sum of radially symmetric spline functions f_h from (4.3) with different centers $\boldsymbol{\zeta}$.

Figure 2a shows a superposition of quadratic splines as defined in Lemma 4.1. This test function will be used throughout the next two sections to illustrate the performance of our reconstruction method for the Funk–Radon as well as for the cosine transform. The reasoning behind the choice of this test function is the following: Firstly, it is not a polynomial. With a polynomial as test function, the aliasing error from (3.11) would vanish if N is sufficiently large, thereby leading to unrealistically good results. Secondly, this test function is an element of the Sobolev space $H^2(\mathbb{S}^2)$, but its second derivative is not continuous. Thirdly, to avoid any possible error caused by a forward algorithm, we have a closed analytic formula for its Funk–Radon transform, which is given in the previous lemma and illustrated in Figure 2b. Note that all spherical plots in this section show even functions, so no information is lost because the backside of the sphere is not visible.

4.3 Numerical results for the inversion of the Funk–Radon transform

First of all we compare the reconstruction with the "optimal" mollifier $\psi_{\tilde{N}}^{s,e}$ from (3.16) with the Dirichlet kernel

$$\psi_{\tilde{N}}^{\mathrm{Dir}} = \sum_{n=0}^{\tilde{N}/2} \frac{4n+1}{4\pi} P_{2n}.$$

In the case of the optimal mollifier, the parameter $\tilde{N}$ is chosen as in (3.17). For the Dirichlet kernel, we used an analogue computation. As sampling points we used a spherical 200-design, which consists of $M = 21\,000$ points $\boldsymbol{\xi}_m \in \mathbb{S}^2$, $m = 1, \dots, M$, and added white noise ε with standard deviation $\sigma = 0.1$ to the Funk–Radon transform $\mathcal{F}f(\boldsymbol{\xi}_m)$ of our test function evaluated at the sampling points. This corresponds to a signal-to-noise ratio of about 2.6 dB.

We also compare our mollifier with the locally supported mollifiers $\psi_{\nu,\gamma}^{\mathrm{loc}}$ introduced in [29]. These are defined for some $\nu \in \mathbb{N}$ and a regularization parameter $\gamma > 0$ by

$$\psi_{\nu,\gamma}^{\mathrm{loc}}(t) = \begin{cases} \frac{1}{e_\nu(\gamma)} \left(1 - \frac{1-t^2}{\gamma^2}\right)^\nu, & t^2 > 1 - \gamma^2 \\ 0, & \text{otherwise,} \end{cases}$$

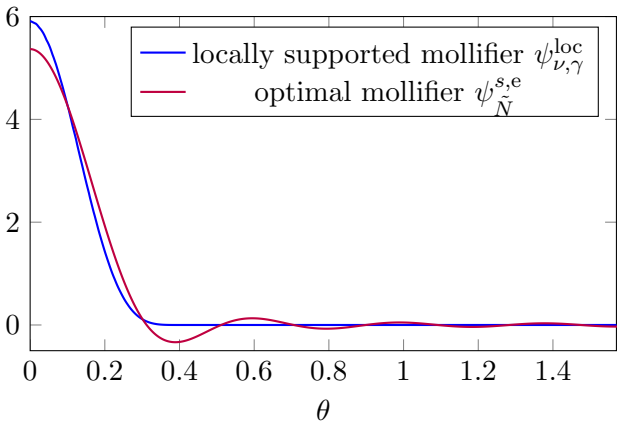

Figure 3: The locally supported mollifier $\psi^{\mathrm{loc}}_{\nu,\gamma}(\cos\theta)$ for $\nu = 5$ and $\gamma = 0.4$, and the even optimal mollifier $\psi^{s,\mathrm{e}}_{\tilde{N}}(\cos\theta)$ for $s = 2$ and $\tilde{N} = 16$.

where the normalization constant $e_\nu(\gamma)$ is chosen such that $\int_{-1}^{1} \psi^{\mathrm{loc}}_{\nu,\gamma}(t)\,\mathrm{d}t = (2\pi)^{-1}$. These mollifiers are illustrated in Figure 3.

The corresponding reconstruction kernels $\Psi^{\mathrm{loc}}_{\nu,\gamma}$ for the Funk–Radon and cosine transform are given explicitly in [29]. Hence, the estimator $\mathcal{E}_{N,\psi^{\mathrm{loc}}_{\nu,\gamma}}$ can be computed directly by (3.1). Thanks to the spherical design $\boldsymbol{\xi}_m \in \mathbb{S}^2$, $m = 1, \dots, M$, we have

$$\mathcal{E}_{N,\psi^{\mathrm{loc}}_{\nu,\gamma}} g(\boldsymbol{\eta}) = \frac{1}{M} \sum_{m=1}^{M} g(\boldsymbol{\xi}_m) \Psi^{\mathrm{loc}}_{\nu,\gamma}(\boldsymbol{\xi}_m \cdot \boldsymbol{\xi}_j), \quad j = 1, \dots, J.$$

However, unlike the mollifiers $\psi^{\mathrm{loc}}_{\nu,\gamma}$, the reconstruction kernels $\Psi^{\mathrm{loc}}_{\nu,\gamma}$ are supported on the whole sphere. As a consequence a direct evaluation of the sum at nodes $\boldsymbol{\eta}_j \in \mathbb{S}^2$, $j = 1, \dots, J$, requires $\mathcal{O}(MJ)$ numeric operations in contrast to the numeric complexity $\mathcal{O}(M \log^2 M + J)$ of the Fourier-based algorithm. This inferior numeric complexity also shows up in the experiments. The reconstruction from $M = 21\,000$ data points and the evaluation at $J \sim M$ nodes takes one second with the Fourier algorithm and 112 seconds with the direct algorithm for the locally supported mollifier on an Intel Core i5-3470 with 8 GB RAM.

Figure 4 compares the reconstructions with the above mentioned mollifiers. As seen in the image, using the optimal mollifier results in a smoother reconstruction that is closer to the original with the exception of the highly-oscillating part (the "blue eyes"). This effect is due to the optimization with respect to the MISE. The maximum error with the Dirichlet kernel is lower, but the L^2–error with the optimal mollifier is lower and the overall impression of the image is better. In Figure 4c, we plotted the reconstruction with the locally supported mollifier $\psi^{\mathrm{loc}}_{\nu,\gamma}$, where we have set $\nu = 5$, which usually yielded good results in [29]. The minimal L^2–error for this method, which is attained for $\gamma = 0.38$, is with 0.0553 comparable to that with the Dirichlet mollifier. Note that, for the locally supported mollifier $\psi^{\mathrm{loc}}_{\nu,\gamma}$, the parameter γ was chosen by numerical optimization, whereas for the optimal parameter $\tilde{N}$ for the mollifier $\psi^{s,\mathrm{e}}_{\tilde{N}}$, formula (3.10) was used.

In the tests we performed, the optical impression of the reconstruction obtained with the locally supported mollifiers $\psi^{\mathrm{loc}}_{\nu,\gamma}$ is usually comparable with the optimal mollifier even though the computed L^2–error is higher. The latter observation can be expected because the optimal

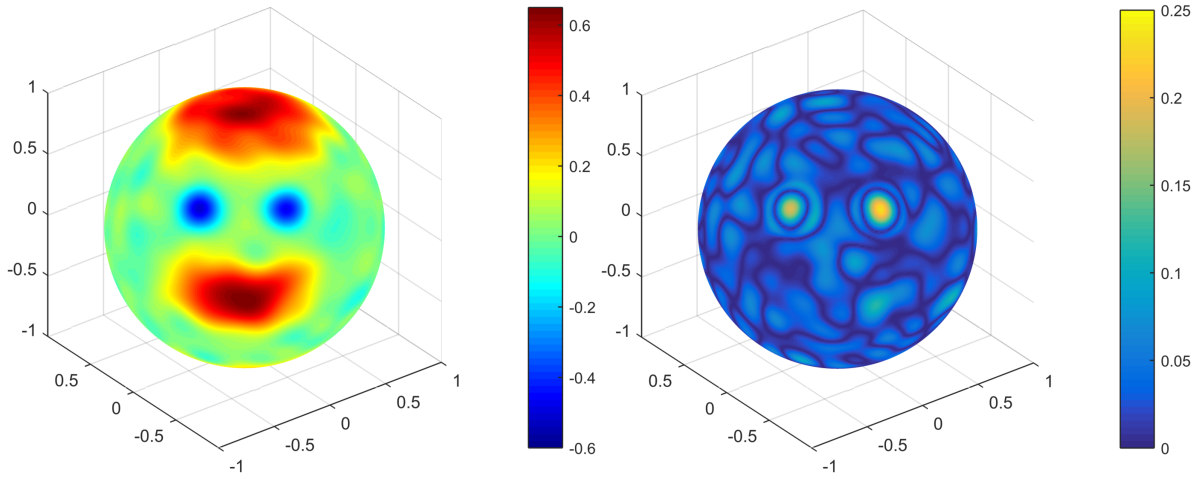

(a) optimal mollifier (relative L^2 error: 0.0277)

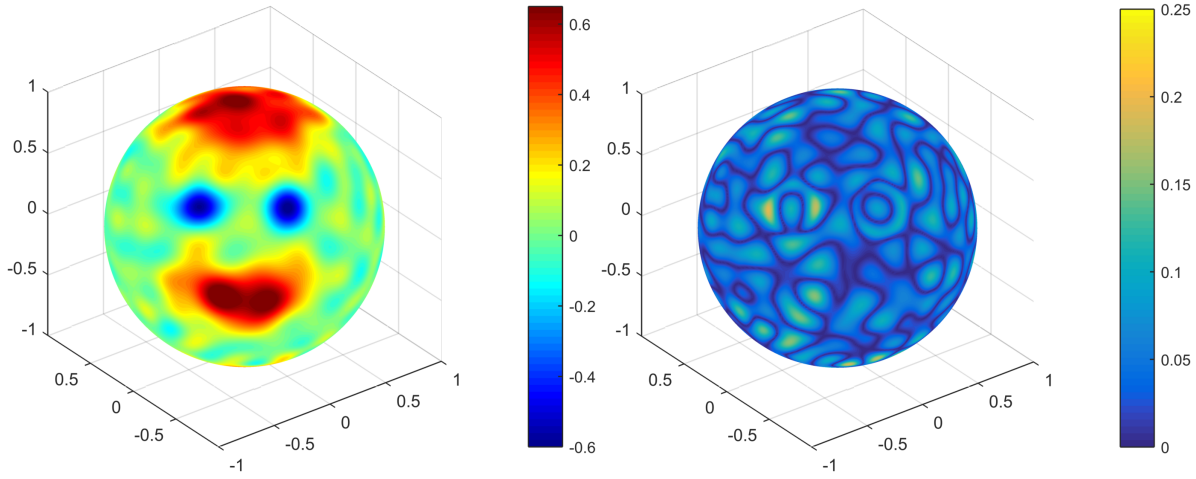

(b) Dirichlet kernel (relative L^2 error: 0.0493)

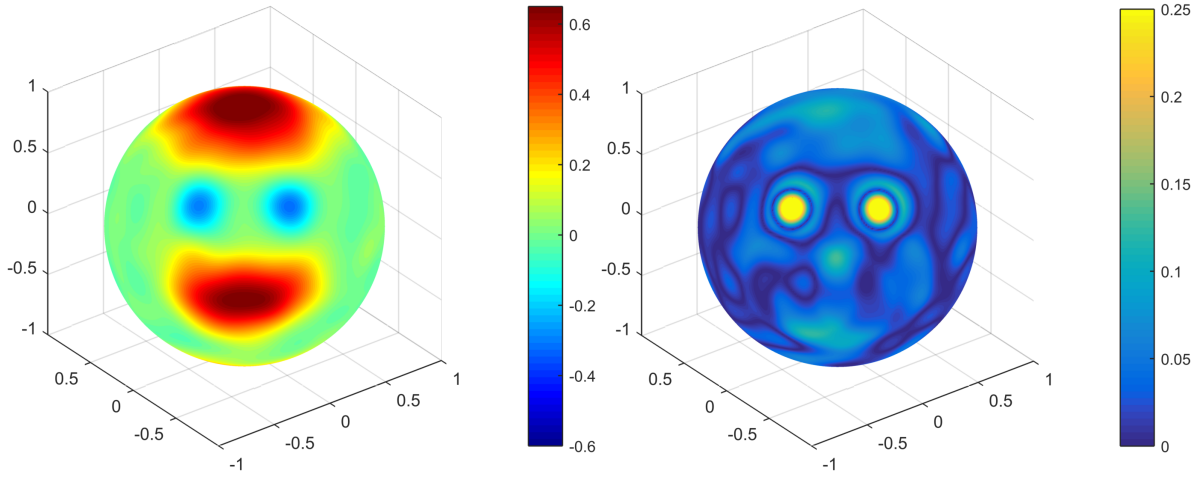

(c) locally supported mollifiers $\psi_{\nu,\gamma}^{\mathrm{loc}}$ with $\gamma = 0.38$ (relative L^2 error: 0.0553)

Figure 4: Reconstruction results $\mathcal{E}_{N,\psi}(\mathcal{F}f + \varepsilon)$ (left) and the respective errors $|f - \mathcal{E}_{N,\psi}(\mathcal{F}f + \varepsilon)|$ (right) from $M = 21\,000$ sampling points with different mollifiers.

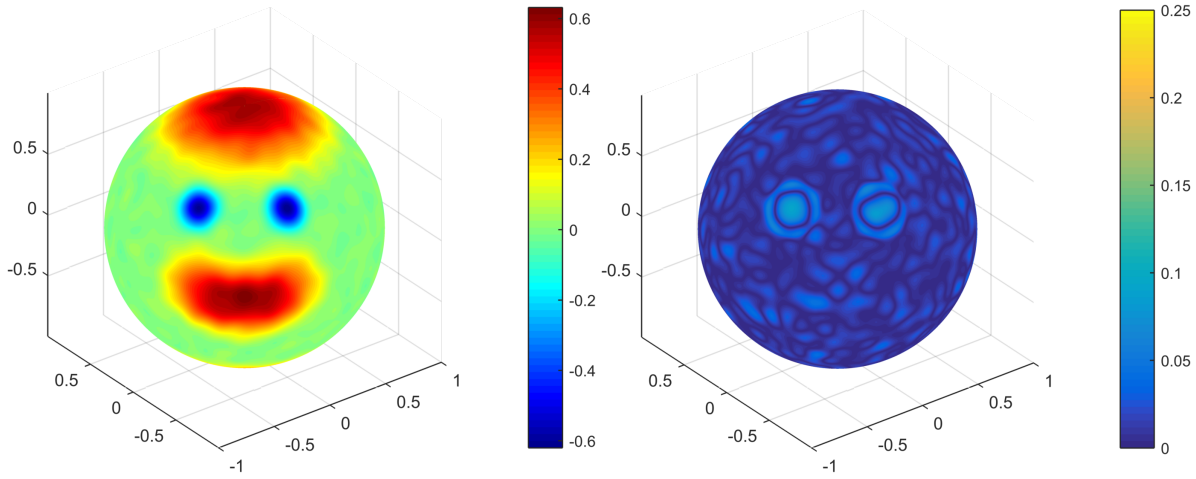

Figure 5: Reconstruction and error with optimal mollifier and $M = 520\,000$ data points

mollifiers minimize the MISE. In the case of only a small number of data available combined with a high noise level, the reconstruction with the locally supported mollifiers $\psi^{\mathrm{loc}}_{\nu,\gamma}$ often looks better, while the L^2–errors are about the same.

Figure 5 shows the reconstruction and the corresponding error with a spherical 1000-design, which consists of 520 000 data points, with the optimal mollifier. This computation takes about five seconds not including the pre-computation needed for the NFSFT.

MISE. Next we want to examine the MISE in dependency of the polynomial degree N and hence the number of sampling points M by following the steps:

i) Choose the function $f \in H^s(\mathbb{S}^2)$, $s = 2$, as defined in the previous section.

ii) Choose a quadrature rule with nodes $\boldsymbol{\xi}_m \in \mathbb{S}^2$, weights $\omega_m \in \mathbb{R}$, $m = 1, \dots, M$, and degree of exactness $2N$.

iii) Fix as the mollifier function $\psi \in L^2(\mathbb{S}^2)$ either the optimal mollifier $\psi^{s,\mathrm{e}}_{\tilde{N}}$ or the Dirichlet kernel $\psi^{\mathrm{Dir}}_{\tilde{N}}$ with optimally chosen $\tilde{N}$ as in (3.17).

iv) Generate a set of point evaluations

$$g_m = \mathcal{M}f(\boldsymbol{\xi}_m) + \varepsilon_m, \quad m = 1, \dots, M,$$

of the Funk–Radon transform, $\mathcal{M} = \mathcal{F}$, perturbed by Gaussian white noise with variance $\sigma = 0.1$.

v) Compute the estimator $\mathcal{E}_{N,\psi}(\mathcal{M}f + \varepsilon)$ at the nodes $\boldsymbol{\xi}_m$, $m = 1, \dots, M$, via the algorithm from the previous section.

vi) Compute the integrated squared error $\|f - \mathcal{E}_{N,\psi}(\mathcal{M}f + \varepsilon)\|^2_{L^2}$ via quadrature.

vii) Compute an estimate of the relative MISE by repeating 20 times the steps iv to vi, taking the mean value of the integrated squared errors and divide it by the L^2–norm of the test function.

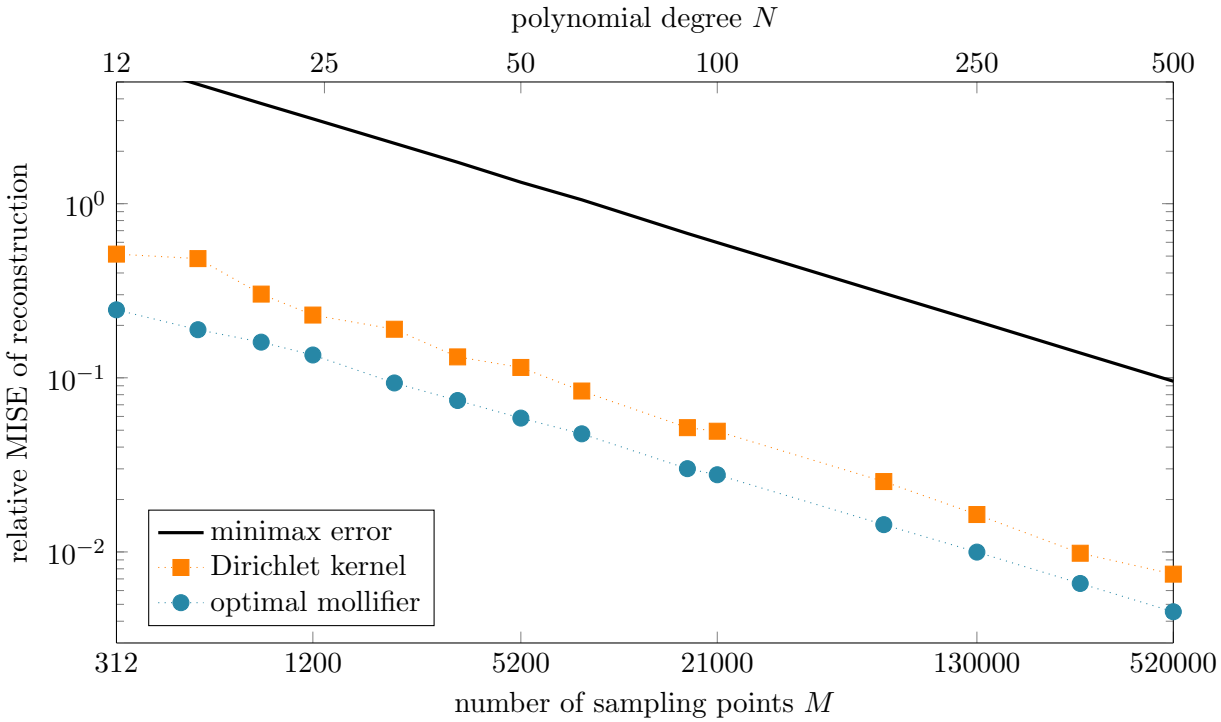

Figure 6: Log–log plot of the relative MISE $\|f - \mathcal{E}(\mathcal{F}f + \varepsilon)\|_{L^2}/\|f\|_{L^2}$ for the reconstruction of the test function f depicted in Figure 2a from its Funk–Radon transform perturbed by white noise ε, signal-to-noise ratio 2.6dB, with respect to the number M of sampling points. The blue circles represent the results using the optimal mollifier $\psi^{s}_{\tilde{N}}$ and the orange squares represent the results using the Dirichlet kernel $\psi^{\mathrm{Dir}}_{\tilde{N}}$. The black line shows the theoretic minimax rate (3.18) for functions within the same Sobolev ball as the test function f.

In Figure 6, we have plotted the relative MISE in dependency of the polynomial degree N and the number of sampling points $M = M(N)$, for the optimal mollifier on the one hand, and for the Dirichlet kernel on the other hand. The diagram shows that the optimal mollifier outperforms the Dirichlet kernel by a factor of almost two in terms of the MISE. The asymptotic rate is the same, but the constant is better for the optimal mollifier. This asymptotic rate is also the same as the one for the theoretically achieved minimax rate. Since the minimax rate is the maximum risk over all functions in the Sobolev ball, it is of course much higher than the actual error for our test function.

Next, we want to examine the optimality of the regularization parameter $\tilde{N}^*$ determined by (3.17) for our specific test function. To this end, we have plotted in Figure 7 the relative MISE, as well as the absolute error in the infinity norm

$$\|f - \mathcal{E}_{N,\psi^{s,\mathrm{e}}_{\tilde{N}}}(\mathcal{F}f + \varepsilon)\|_{L^\infty} = \max_{\mathbb{S}^2} \left| f - \mathcal{E}_{N,\psi^{s,\mathrm{e}}_{\tilde{N}}}(\mathcal{F}f + \varepsilon) \right|,$$

for $N = 500$ and $\tilde{N} = 2, 4, \ldots, 100$. We observe the typical convex shape with minimum attained at $\tilde{N} \approx 38$, which is quite close to the value $\tilde{N}^* \approx 39.9146$ derived from (3.17).

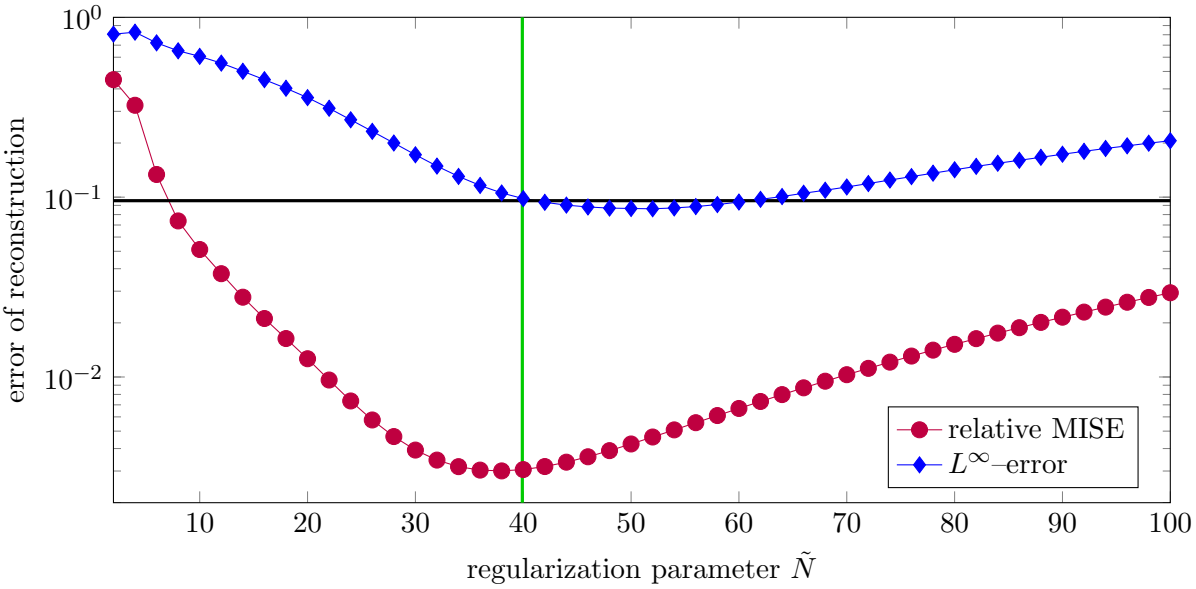

Figure 7: Error of the reconstruction from $M = 520\,000$ data points ($N = 500$) with respect to the regularization parameter $\tilde{N}$. The green line indicates the computed value $\tilde{N}^*$ from (3.17). The black line indicates the minimax (3.18) of the relative MISE for $\tilde{N} = \tilde{N}^*$.

4.4 Numerical results for the inversion of the cosine transform

For the spherical cosine transform we apply the same testing procedure as for the Funk–Radon transform. The cosine transform of the test function from the previous section perturbed by Gaussian white noise with standard deviation $\sigma = 0.01$, which corresponds to a signal-to-noise ratio of about 21 dB, is depicted in Figure 8a. Figure 8b shows the reconstruction from $M = 520\,000$ data points and with polynomial degree $N = 500$. We observe stronger artifacts compared to the reconstruction from the Funk–Radon transform, which are due to the higher ill-posedness of the inversion of the cosine transform. Nonlinear estimators with stronger reference to the smoothness of the test function would probably do a better job here.

A comparison of the achieved relative MISE for the cosine transform with the minimax rate from (3.19) is illustrated in Figure 9. The MISE has a similar behavior as for the Funk–Radon transform even though it is on a higher level.

Acknowledgments

We would like to express our thanks to Manuel Gräf, who has provided the approximate spherical designs we used for testing our algorithm.

References

[1] F. Bauer and M. A. Lukas. Comparing parameter choice methods for regularization of ill-posed problems. *Math. Comput. Simulation*, 81(9):1795–1841, May 2011.

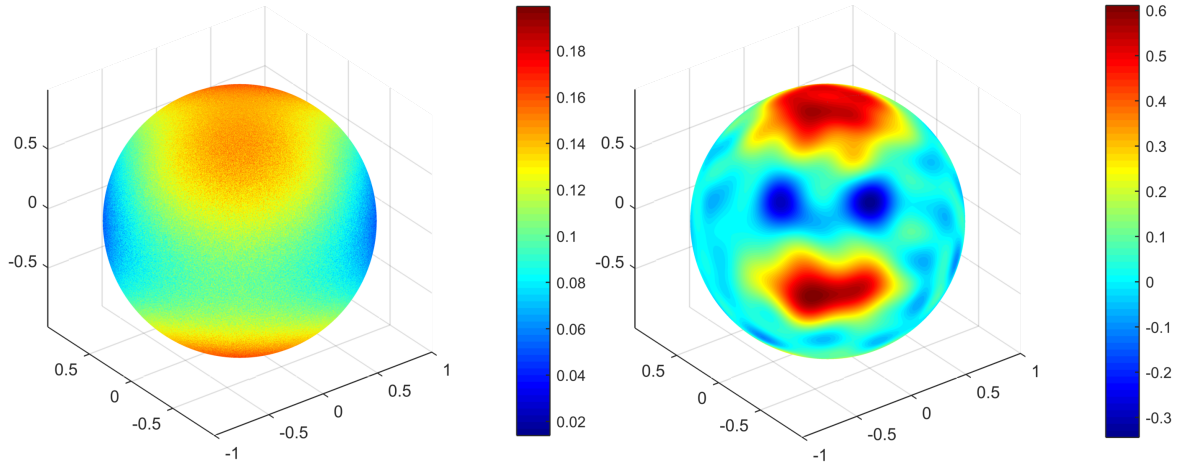

(a) $\mathcal{C}f + \varepsilon$ (b) Reconstruction

Figure 8: Cosine transform of the function from Figure 2a and its reconstruction. The left image shows the cosine transform with added random noise ε that has a variance of $\sigma = 0.01$ and the right image the reconstruction given from $M = 520\,000$ data points.

[2] A. Bondarenko, D. Radchenko, and M. Viazovska. Optimal asymptotic bounds for spherical designs. *Ann. of Math.*, 178(2):443–452, 2013.

[3] S. Campi. On the reconstruction of a star-shaped body from its half-volumes. *J. Austral. Math. Soc. Ser. A*, 37(02):243 – 257, 1984.

[4] L. Cavalier. Nonparametric statistical inverse problems. *Inverse Problems*, 24(3):034004, June 2008.

[5] F. Dai and Y. Xu. *Approximation theory and harmonic analysis on spheres and balls.* Springer Monographs in Mathematics. Springer, New York, 2013.

[6] F. Filbir and H. Mhaskar. A quadrature formula for diffusion polynomials corresponding to a generalized heat kernel. *J. Fourier Anal. Appl.*, 16:629 – 657, 2010.

[7] W. Freeden, T. Gervens, and M. Schreiner. *Constructive Approximation on the Sphere.* Oxford University Press, Oxford, 1998.

[8] P. Funk. Über Flächen mit lauter geschlossenen geodätischen Linien. *Math. Ann.*, 74(2):278 – 300, June 1913.

[9] P. Funk. Über eine geometrische Anwendung der Abelschen Integralgleichung. *Mathematische Annalen*, 77:129 – 135, 1915.

[10] R. J. Gardner. *Geometric tomography.* Number 58 in Encyclopedia of Mathematics and its Applications. Cambridge University Press, Cambridge; New York, second edition, 2006.

[11] E. Gautier and Y. Kitamura. Nonparametric estimation in random coefficients binary choice models. *Econometrica*, 81(2):581–607, 2013.

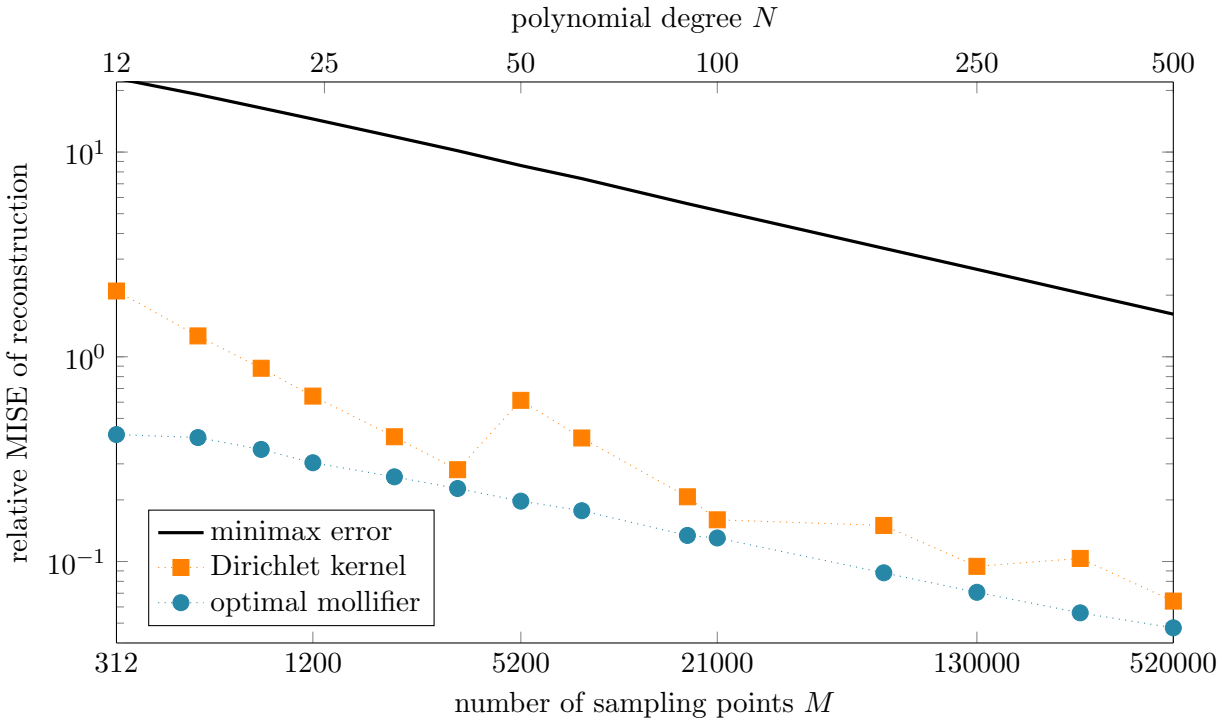

Figure 9: Log–log plot of the relative MISE $\|f - \mathcal{E}(\mathcal{C}f + \varepsilon)\|_{L^2}/\|f\|_{L^2}$ for the reconstruction of the test function f depicted in Figure 2a from its cosine transform perturbed by white noise ε, signal-to-noise ratio 21dB, with respect to the number M of sampling points. The blue circles represent the results using the optimal mollifier $\psi_{\tilde{N}}^{s,\mathrm{e}}$ and the orange squares represent the results using the Dirichlet kernel $\psi_{\tilde{N}}^{\mathrm{Dir}}$. The black line shows the theoretic minimax rate (3.19) for functions within the same Sobolev ball as the test function f.

[12] P. Goodey and W. Weil. Centrally symmetric convex bodies and the spherical Radon transform. *J. Differential Geom.*, 35(3):675–688, 1992.

[13] M. Gräf and D. Potts. On the computation of spherical designs by a new optimization approach based on fast spherical Fourier transforms. *Numer. Math.*, 119:699 – 724, 2011.

[14] S. Helgason. *The Radon Transform.* Birkhäuser, 2nd edition, 1999.

[15] K. Hesse and I. H. Sloan. Hyperinterpolation on the sphere. In N. K. Govil, H. N. Mhaskar, R. N. Mohapatra, Z. Nashed, and J. Szabados, editors, *Frontiers in Interpolation and Approximation*, Pure and Applied Mathematics. Taylor & Francis Books, Boca Raton, Florida, 2006.

[16] P. Jonas and A. K. Louis. A Sobolev space analysis of linear regularization methods for ill-posed problems. *J. Inverse Ill-Posed Probl.*, 9(1):59 – 74, 2001.

[17] J. Keiner and D. Potts. Fast evaluation of quadrature formulae on the sphere. *Math. Comput.*, 77:397 – 419, 2008.

[18] M. Kiderlen and A. Pfrang. Algorithms to estimate the rose of directions of a spatial fiber system. *J. Microsc.*, 219(2):50–60, Aug. 2005.

[19] P. T. Kim and J. Koo. Optimal spherical deconvolution. *J. Multivariate Anal.*, 80:21 – 42, 2002.

[20] S. Kunis and D. Potts. NFFT, Softwarepackage, C subroutine library, 2002 – 2006.

[21] S. Kunis and D. Potts. Fast spherical Fourier algorithms. *J. Comput. Appl. Math.*, 161:75 – 98, 2003.

[22] S. Kunis and D. Potts. Time and memory requirements of the nonequispaced FFT. *Sampl. Theory Signal Image Process.*, 7:77 – 100, 2008.

[23] A. K. Louis and P. Maass. A mollifier method for linear operator equations of the first kind. *Inverse Problems*, 6(3):427–440, June 1990.

[24] A. K. Louis, M. Riplinger, M. Spiess, and E. Spodarev. Inversion algorithms for the spherical Radon and cosine transform. *Inverse Problems*, 27(3):035015, Mar. 2011.

[25] C. Müller. *Spherical Harmonics.* Springer, Aachen, 1966.

[26] I. Pesenson. Variational splines on Riemannian manifolds with applications to integral geometry. *Adv. in Appl. Math.*, 33:548 – 572, 2004.

[27] I. Z. Pesenson and D. Geller. Cubature formulas and discrete Fourier transform on compact manifolds. In H. M. Farkas, R. C. Gunning, M. I. Knopp, and B. A. Taylor, editors, *From Fourier Analysis and Number Theory to Radon Transforms and Geometry*, volume 28 of *Developments in Mathematics*, pages 431–453. Springer New York, 2013.

[28] C. M. Petty. Centroid surfaces. *Pacific J. Math.*, 11:1535–1547, Dec. 1961.

[29] M. Riplinger and M. Spiess. Numerical inversion of the spherical Radon transform and the cosine transform using the approximate inverse with a special class of locally supported mollifiers. *J. Inverse Ill-Posed Probl.*, 22(4):497 – 536, Dec. 2013.

[30] H. Robbins. A remark on Stirling's formula. *Amer. Math. Monthly*, pages 26–29, 1955.

[31] B. Rubin. Inversion of fractional integrals related to the spherical Radon transform. *J. Funct. Anal.*, 157(2):470 – 487, Aug. 1998.

[32] B. Rubin. Inversion and characterization of the hemispherical transform. *J. Anal. Math.*, 77(1):105 – 128, 1999.

[33] B. Rubin. Inversion formulas for the spherical Radon transform and the generalized cosine transform. *Adv. in Appl. Math.*, 29(3):471 – 497, 2002.

[34] D. S. Tuch. Q-ball imaging. *Magn. Reson. Med.*, 52(6):1358–1372, Nov. 2004.

[35] C. E. Yarman and B. Yazici. Inversion of the circular averages transform using the Funk transform. *Inverse Problems*, 27(6):065001, June 2011.